Measurement 219 (2023) 113276

Contents lists available at ScienceDirect

Measurement

journal homepage: www.elsevier.com/locate/measurement

Experimental evaluation and numerical interpretation of various noise mitigation strategies for in-service elevated suburban rail

Yun-Ke Luo [a,b], Li-Zhong Song [c,d], Chao Zhang [a,b], Yi-Qing Ni [a,b,*]

[a] Department of Civil and Environmental Engineering, The Hong Kong Polytechnic University, Hung Hom, Kowloon, Hong Kong Special Administrative Region
[b] Hong Kong Branch of National Rail Transit Electrification and Automation Engineering Technology Research Center, Hung Hom, Kowloon, Hong Kong Special Administrative Region
[c] State Key Laboratory of Performance Monitoring and Protecting of Rail Transit Infrastructure, East China Jiaotong University, Nanchang, China
[d] MOE Engineering Research Center of Railway Environmental Vibration and Noise, East China Jiaotong University, Nanchang, China

ARTICLE INFO

Keywords:
Elevated suburban rail
Noise control
Experimental evaluation
Numerical interpretation
Noise barrier
Rolling noise
Bridge-borne noise

ABSTRACT

This research evaluates the efficiency of five noise mitigation measures including rubber floating slab track, straight noise barrier, track acoustic absorber, track-side noise barrier, semi-closed noise barrier, and a combined strategy on an elevated railway through in-situ measurements. In-situ experiments were conducted by sequentially installing various mitigation measures for comparative evaluation. A numerical model was then developed to interpret the noise control characteristics of the mitigation measures. The experimental results indicate that the rubber floating slab track can mitigate bridge-borne noise by 0-4 dB sound pressure level (SPL); the track acoustic absorber can mitigate the railway noise by 3–5 dB(A) and its combination with track-side noise barrier boosts the insertion losses of SPL by 2–7 dB(A). The combined control strategy shows overall better performance than individual mitigation measures within the efficient noise reduction regions. The experimental and numerical results can serve as a guide on the design of noise control strategies for elevated railways.

1. Introduction

Suburban rail on elevated bridges is a relatively economic and environment-friendly type of rapid rail transit. Compared with underground railways, its construction unit cost can be greatly reduced [1]; moreover, the working environment for maintenance and structural condition evaluation is much more accessible. On the other hand, however, the elevated suburban rail is more susceptible to noise because it will inevitably pass through those noise-sensitive areas, such as schools, hospitals, and residential regions. As reported in [2], persistent high-level noise exposure leads to the impairment of human's spirit and reduction of working and studying efficiency, and will also potentially harm vibration-sensitive precision instruments. Thus, adequate noise and vibration control strategies must be implemented without sacrificing economic efficiency.

Train-induced noise and vibration have been an important research field due to the complexity of railway-related acoustic mechanisms and the coupled dynamic behaviors among train, track, bridge and subgrade [3]. According to [4], railway noise sources can be in general categorized into wheel-rail rolling noise [5,6], wheel-rail squeal noise [7–10], structure-borne noise [11,12], aerodynamic noise [13], and ground-borne vibration and noise [14–16]. Among them, wheel-rail rolling noise and structure-borne noise tend to be predominant for general elevated rail transit operating at speeds below 150 km/h [4]. The rolling noise consists of a relatively high frequency component ranging between 500 Hz and 2000 Hz [17] and is mainly caused by the rolling contact between the wheel and the rail. Rail surface roughness was found to be one of the paramount excitation sources of rolling noise [18]. In terms of the noise contribution, both wheel and rail were reported to be equally important in radiating the rolling noise above 1250 Hz, while the rail tends to be a more predominant source for frequencies below 1250 Hz [19]. These characteristics suggest that the design of rolling noise mitigation measures should be in connection with the frequency range. Mitigation measures such as rail damper, wheel damping layer, noise barrier, bogie shroud, etc., have been proposed for this target by considering the frequency properties [20]. The structure-borne noise or more specifically, the bridge-borne noise, on the contrary, contains overall lower frequency components than the rolling noise.

* Corresponding author at: Department of Civil and Environmental Engineering, The Hong Kong Polytechnic University, Hung Hom, Kowloon, Hong Kong Special Administrative Region.
E-mail address: ceyqni@polyu.edu.hk (Y.-Q. Ni).

https://doi.org/10.1016/j.measurement.2023.113276
Received 24 January 2023; Received in revised form 19 May 2023; Accepted 30 June 2023
Available online 1 July 2023

Fig. 1. Site conditions of (a) straight barrier section, (b) semi-closed barrier section for unmodified test section, and (c) track-side barrier at controlled test section.

Predominant frequency bands were reported below 1000 Hz for steel bridges [21–23] and between 20 Hz and 200 Hz for concrete bridges [24–26]. Mitigation measures, such as additional damping layer of bridges [27], rail dampers [22], soft rail pads [28], and resilient fasteners [29], etc., were reported to be effective in mitigating the bridge-borne noise.

While a wide range of noise mitigation measures have been proposed and applied in engineering practice in the light of various circumstances, such as rail dampers for rolling noise below 1000 Hz [20], and resilient fasteners isolating vibration for reduction of bridge-borne noise [29], it is highly desirable to compare the performance of diverse noise control strategies under same operating conditions and to validate the efficiency of the implemented noise control measures through in-situ experiments. Apart from fully taking account of the complexity and variability of a railway acoustic system in practical application, in-situ experiments can also remedy the weakness in design stage stemming from simplified models and ignored factors. Conducting railway acoustic measurements by deploying a large number of sensors and monitoring instruments in consideration of various mitigation measures is the most straightforward way to evaluate the effectiveness of the implemented noise control measures. However, it is rarely a general noise control workflow because of being highly expensive and time-consuming when applied to a suburban rail line typically with dozens of kilometers. In view of this, selecting several representative test sections and calibrating numerical models for the tested sections would be more feasible for developing noise radiation and control prediction models which can be generalized to the whole rail line for guiding the selection/implementation of noise mitigation measures to achieve the targeted control efficiency. The commonly used simulation strategies to develop numerical models for this purpose include the boundary element method (BEM) [30] for low frequency bridge-borne noise [31,32] and the statistical energy analysis (SEA) [33] for high frequency rolling noise and steel bridge noise [11,34]. A hybrid simulation strategy, where the BEM is used for bridge-borne noise while the SEA is used for wheel-rail rolling noise, will be employed in this study to achieve versatility and adaptability in numerical modelling.

The primary goal of this study is to comparatively evaluate the efficiency and adaptability of five typical noise and vibration mitigation measures, including rubber floating slab track, track acoustic absorber, straight noise barrier, track-side noise barrier, semi-closed noise barrier, and a combined control strategy, by successively deploying them on an in-service elevated suburban rail and conducting experimental verification. Well-controlled in-situ experiments with the same model of trains travelling on the rail are conducted to ensure consistency in the operating conditions and comparability of measurement results. Based on the measurements, numerical models for the tested sections are established and calibrated. The calibrated models are then applied to carry out component-by-component analysis for each noise and vibration mitigation measure and to interpret the efficiency of individual and combined control strategies. The major contributions of this investigation include:

- Recommendations on how to select/implement efficient noise mitigation measures, and the corresponding experimental and numerical justifications;
- An insight into the noise reduction characterizations of different noise mitigation measures under in-service conditions; and
- A guide on the selection of adequate noise control strategies for new elevated railways with similar structural properties.

This article is organized as follows. Section 2 presents the details of in-situ experiments. The efficiency of five noise and vibration mitigation measures and a combined strategy is comparatively evaluated. Model development and calibration procedures are described in section 3. Section 4 provides the simulation results in line with the measurement conditions, and compares the numerical and experimental results. Section 5 summarizes the experimental evaluation and numerical interpretation and draws conclusions.

2. In-situ experiments

This section describes the design of in-situ experiments on an in-service suburban rail. Three unmodified test sections and one controlled test section with several noise control strategies were included. The three unmodified test sections are a standard section without any noise and vibration control measure, a straight barrier section with a single-side noise barrier and rubber floating slab track, and a noise-sensitive section with semi-closed noise barrier and rubber floating slab track. The controlled test section was initially equipped with rubber floating slab track; track acoustic absorber and track-side noise barrier were then sequentially installed to form combined noise control strategies. A total of seven measurements were carried out during the passage of the same model of train vehicles, and tests under various running speeds were specifically conducted for the controlled test section and the standard section. The measurement results are analyzed to make a comparative experimental evaluation on the vibration control performance of the rubber floating slab track, and the noise control efficiency of the other measures.

2.1. Experiment setup

2.1.1. Noise and vibration mitigation measures

Five noise and mitigation measures are included in this in-situ experiment, which are rubber floating slab track, straight barrier, semi-closed barrier, track-side barrier, and track acoustic absorber.

Noise barrier is a widely used railway noise control method [35]. It

Fig. 2. (a) Rubber floating slab track, (b) track acoustic absorber, and (c) combined rubber floating slab track, absorber, and track-side barrier.

Table 1
Measurement sections and operating conditions.

35 m simply supported box-girder bridge	
Section	**Speed (km/h)**
Unmodified test section	
Standard	40, 60, 100
Straight barrier	100
Semi-closed barrier	60
Controlled test section	
Rubber floating slab track	40, 60
Track acoustic absorber	40, 60
Track-side barrier	40, 60
Absorber and barrier	40, 60

blocks the direct path of noise waves from railway noise sources to the nearby receivers. Rubber seals are installed between unit plates of noise barriers to maintain a good sealing condition. Specially designed barrier surfaces will further help reduce noise wave propagation [36]. Fig. 1(a) is the straight barrier section. This barrier is 3.73 m high from the rail head plane, and 3.17 m away from the adjacent track central line; Fig. 1 (b) is the semi-closed barrier section. The total height of the semi-closed barrier is 7.3 m from the rail head plane, and the lateral length of top rubber plate is 6.38 m, which has fully covered one side of the double-track railway line. The barrier is also installed 3.17 m away from the adjacent track central line; Fig. 1(c) is the track-side barrier. This kind of barrier is lower but closer to the train vehicle. The track-side barrier is 0.94 m high from the rail head plane, and 1.95 m away from the adjacent track central line. The thickness of each unit plate of the above noise barriers is around 150 mm.

Fig. 2(a) is the rubber floating slab track section. The rubber floating slab track is designed mainly to mitigate low frequency vibration of the bridge structure and ground by installing a rubber layer inside the track plate [37]. The rubber layer has much lower stiffness and thus isolates the vibration energy from the rail [38–40]. However, the isolated energy will not disappear, instead, it maintains in the rail and wheels. As a result, the use of rubber floating slab track in general will accompany some other noise mitigation measures to reduce the increased wheel-rail noise component. Fig. 2(b) is the track acoustic absorber. The absorber is made of a porous material that traps acoustic waves. Fig. 2(c) is the combined strategy of rubber floating slab track, track acoustic absorber, and track-side noise barrier. This combined strategy can theoretically make benefits from different noise mitigation measures. A better noise reduction performance is expected.

2.1.2. Test condition and sensor arrangement

The standard section serves as a baseline to evaluate the vibration control performance of the rubber floating slab track, and the noise mitigation efficiency of straight barrier and semi-closed noise barrier. The controlled test section is equipped with rubber floating slab track, which is regarded as the initial state for this section. Then, track acoustic absorber and track-side barrier are subsequently installed on the section. Cross comparison between the standard section and the controlled test section under its initial state is considered as a reference for assessing the performance of rubber floating slab track in mitigating the bridge vibration and bridge-borne noise.

The measurement sections and train operating conditions are summarized in Table 1. It should be noted that the operating speeds at the unmodified test sections except for the standard section, follow the in-service operating train speeds. Measurements were conducted on normal train passages in the afternoon. Data of more than 5 train passages was collected for each section. The controlled test section was conducted at speeds of 40 km/h and 60 km/h, while the standard section was tested at speeds of 40 km/h, 60 km/h, and 100 km/h, both using a single train vehicle specifically selected for the tests at midnight. All speed-controlled tests were carried out with three repetitive runs to ensure data reliability. The train used in this study is a Chinese Type D model with four cars. Each car is 22 m in length and 3.3 m in width. The traction motor is located on the second and third cars. During the measurement period for the unmodified test sections (except for the standard section), only a small number of passengers were on board. For the speed-controlled test sections, there were no passengers on board.

Fig. 3 shows the tested suburban train, synchronized data acquisition system, setup of one single microphone array at the measurement site, and the accelerometer and microphone installed under the bridge. Fig. 4 shows the measuring points that were arranged consistently in all test sections. A total of twelve free-field microphones (Type 4939, B&K Ltd., M1-M12), named distributed microphone array, were deployed within one cross-section to capture the radiated railway noise. Two more microphones (MB1, MB2) and two accelerometers (VB1, VB2) were installed under the bridge, aiming to capture both bridge vibration and bridge-borne noise. Both the acoustic and acceleration measurement data were collected using a 16-Channel datalogger (SIRIUS DAQ, Dewesoft, d.o.o.) to ensure data synchronization.

In the in-situ experiments, efforts have been made to ensure general consistency in terms of measuring source-to-sensor distances and devices, structural parameters (e.g., bridge type as a simply supported bridge of 35 m long, sleeper type), train parameters (same train vehicle type), weather condition (without raining). However, it is also important to acknowledge that noise level differences caused by different track locations due to uncertainties are likely to exist for unmodified measurement sections and cannot be fully eliminated [41]. Different track locations may slightly influence the resultant insertion losses of the mitigation measures, while such a condition also reflects the most realistic in-service performances of various measures, which cannot be realized in a fully controlled laboratory benchmark test. Therefore, the direct comparisons among different sections and the resulting insertion

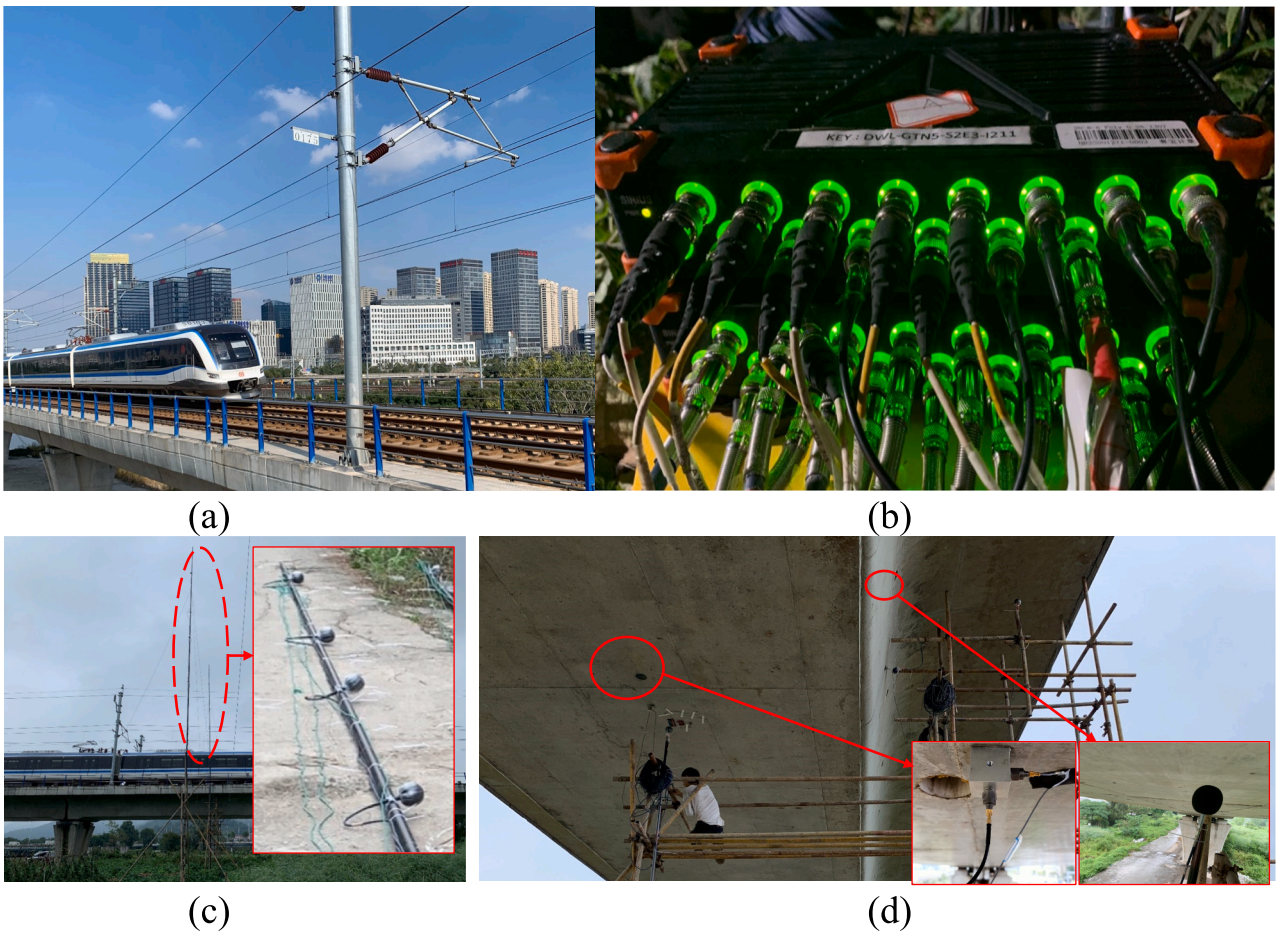

Fig. 3. (a) Suburban train, (b) data acquisition system, (c) setup of one microphone array, and (d) setup of microphone and accelerometer under the bridge.

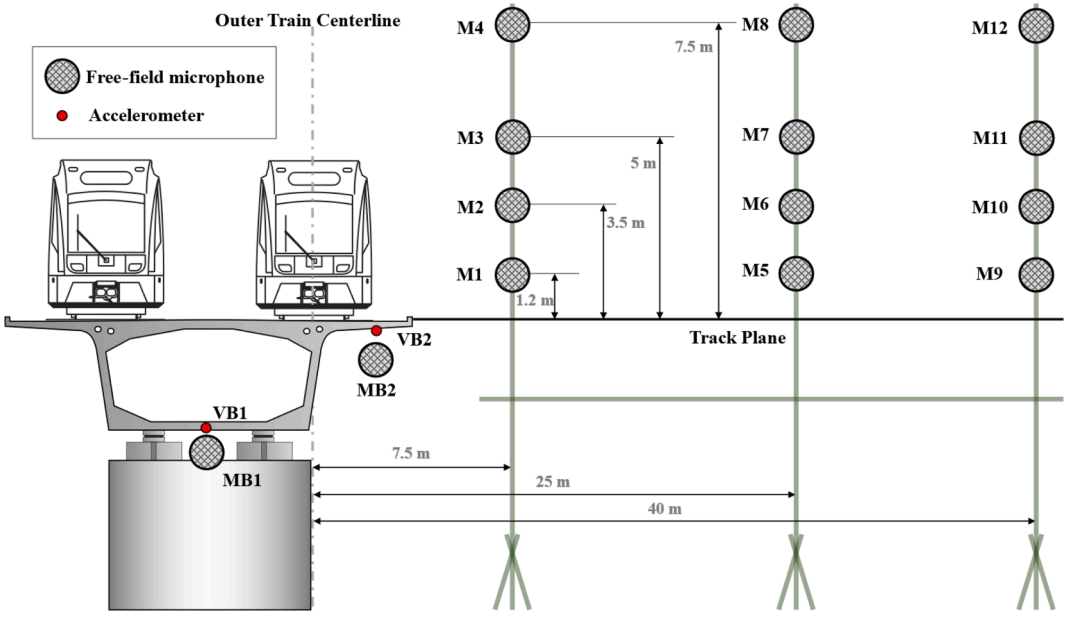

Fig. 4. Implementation locations of the measurement system.

losses from different strategies hold enough guiding significance for the railway authority. Moreover, the comparisons made on the controlled test section with successive additions of mitigation measures at a single track location are considered to be more straightforward. In light of this, we have classified the two sets of sections as “unmodified test section” and “controlled test section” to point out this setup difference.

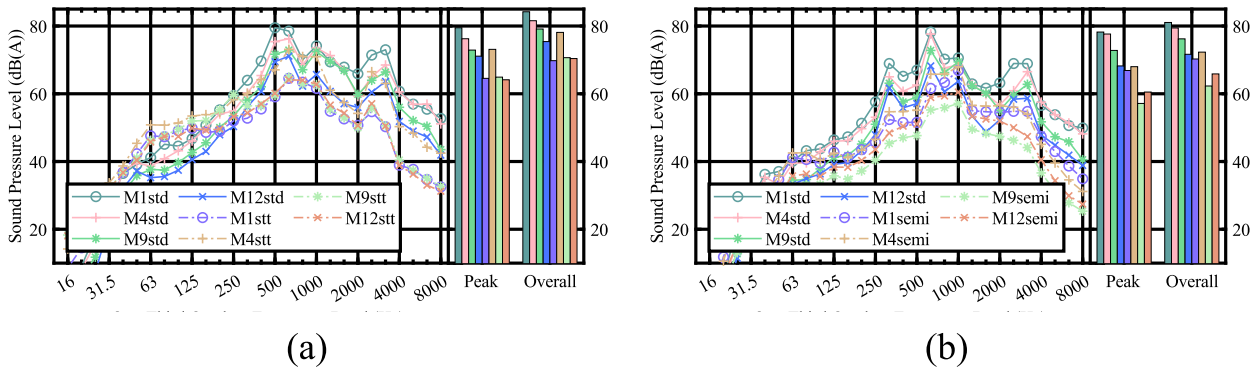

Fig. 5. SPL comparisons of standard section with (a) straight barrier at 100 km/h and (b) semi-closed barrier at 60 km/h. (std: standard section; stt: straight barrier section; semi: semi-closed barrier section).

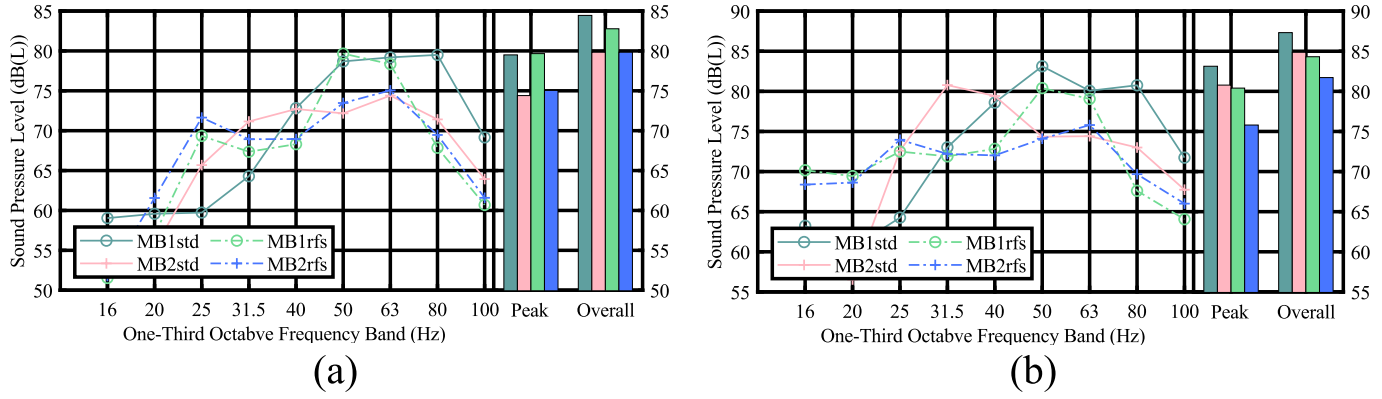

Fig. 6. SPL (linear) comparisons of standard section with rubber floating slab track at (a) 40 km/h and (b) 60 km/h. (std: standard section; rfs: rubber floating slab track section).

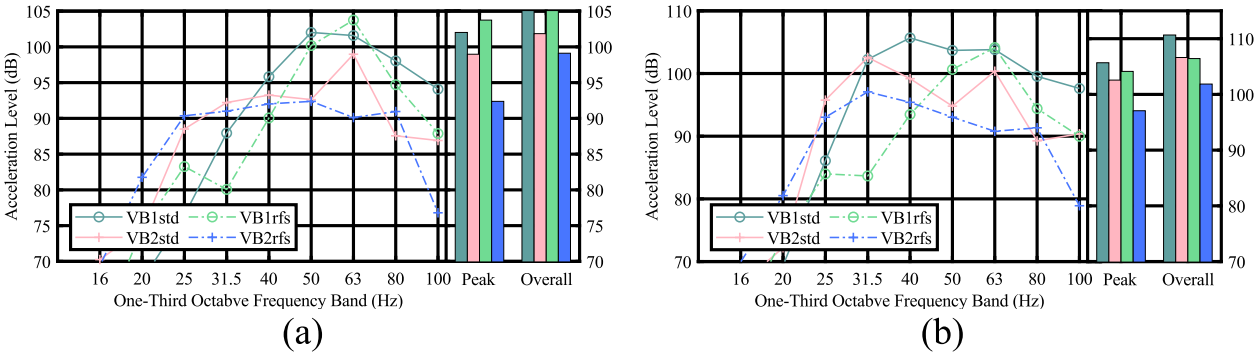

Fig. 7. VAL comparisons of standard section with rubber floating slab track at (a) 40 km/h and (b) 60 km/h. (std: standard section; rfs: rubber floating slab track section).

2.2. Measurements and evaluations

Two direct comparisons are conducted: one is on the unmodified test sections and the other on the controlled test section. To avoid redundant presentation for measuring points with similar values, data collected by microphones located at the array boundaries (M1, M4, M9, M12) are selected for the direct comparisons. An additional cross comparison between the standard section and the controlled test section with only rubber floating slab track is carried out as an extra reference for evaluating the performance of the rubber floating slab track in mitigating the bridge vibration and bridge-borne noise. To eliminate the influence of train speed, the evaluation for straight barrier and semi-closed barrier is made with operating speeds of 100 km/h and 60 km/h, respectively. A detailed comparison is conducted on the controlled test section, where the evaluation is processed at two operating speeds of 40 km/h and 60 km/h. A cross comparison between the two sections is presented at last with operating speeds of 40 km/h and 60 km/h.

Fig. 5(a) shows the noise mitigation efficiency of the straight barrier (3.5 m height and 3.2 m away from the track center). Intuitively, the most efficient noise mitigation area of a straight barrier should not exceed the barrier height. In the measurement, the highest insertion loss is 14 dB(A), which is found at the measuring point M1. The measurement points M4 and M9 above the straight barrier show worse mitigation efficiency with insertion loss of around 5 dB(A). Fig. 5(b) provides the comparison results between the standard section and the semi-closed barrier section under 60 km/h. Similar to the noise mitigation feature of

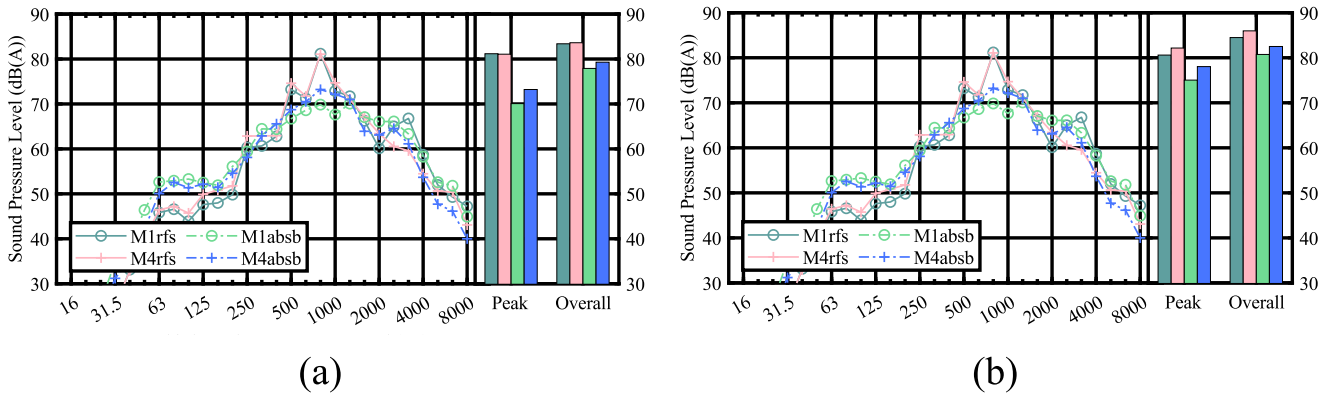

Fig. 8. SPL comparisons of rubber floating slab track with track acoustic absorber at controlled test section: (a) 40 km/h and (b) 60 km/h. (rfs: rubber floating slab track section; absb: track acoustic absorber).

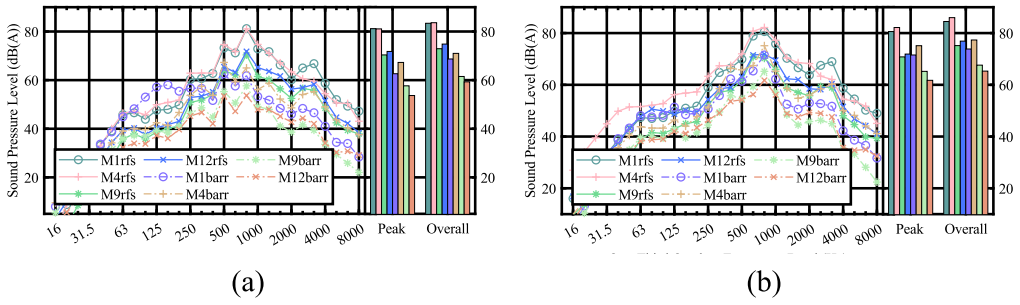

Fig. 9. SPL comparisons of rubber floating slab track with track-side barrier at controlled test section: (a) 40 km/h and (b) 60 km/h. (rfs: rubber floating slab track section; barr: track-side noise barrier).

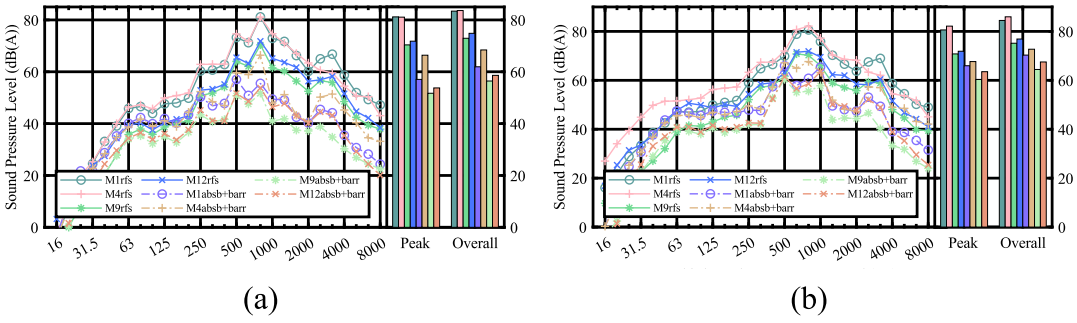

Fig. 10. SPL comparisons of rubber floating slab track with track absorber combined with track-side barrier at controlled test section: (a) 40 km/h and (b) 60 km/h. (rfst: rubber floating slab track section; absb + barr: track acoustic absorber combined with track-side noise barrier).

the straight barrier, larger insertion losses are found at the lower region (M1, M9) as 11 dB(A) and 14 dB(A), respectively. As for the measuring points at 7.5 m above the track plane (M4, M12), insertion losses become 7 dB(A) and 6 dB(A), which do not show much better performance than the straight barrier does. This similar performance may be attributed to the limited height of sensors' deployment. Also, a question arises as to whether the semi-closed noise barrier holds enough capacity in mitigating railway noise for elevated rail in the vicinity of high-rise buildings when considering its extremely high construction and maintenance costs. If not, the semi-closed noise barrier will not be preferable due to its similar performance as the straight noise barrier.

Fig. 6 and Fig. 7 show the linear sound pressure level (SPL(L)) and vibration acceleration level (VAL) between the standard section and the rubber floating slab track section, aiming to evaluate the performance of rubber floating slab track in mitigating the bridge vibration and noise. It is observed that the rubber floating slab track shows a moderate mitigation efficiency for both bridge vibration and bridge-borne noise, with insertion losses as 1–5 dB VAL and 0–4 dB(L) SPL. A better mitigation efficiency is found at higher operating speeds.

Comparisons among the controlled test section with different mitigation measures are presented in Figs. 8–10. The rubber floating slab track scenario is regarded as a baseline for evaluation. In Fig. 8, due to the site limitation during the experiments, only two measuring points (M1, M4) were arranged and thus the noise mitigation efficiency of track acoustic absorber can only be roughly estimated from the two sensors. The track acoustic absorber is found to provide a 5 dB(A) insertion loss at 40 km/h and 3 dB(A) at 60 km/h. The mitigation efficiency estimated from the different sensors seems consistent, though more evidence is needed.

Mitigation efficiency of track-side barrier (0.94 m height) is presented in Fig. 9. This kind of noise barrier is deployed much closer to the wheel and rail (1.9 m from the nearest track central line) than a regular straight barrier does (3.2 m from the nearest track central line), and therefore, may provide a larger efficient noise reduction region. At 40

Table 2
Summary of measurements and evaluation results.

Section	Speed (km/h)	Measuring points	Peak SPL (dB(A) for M1, M4, M9, M12 and dB for MB1, MB2)/Peak VAL (dB) for VB	Overall SPL (dB(A) for M1, M4, M9, M12 and dB for MB1, MB2)/Peak VAL (dB) for VB	Insertion loss: SPL (dB(A) for M1, M4, M9, M12 and dB for MB1, MB2)/VAL (dB) for VB
Standard	40	M1	78@(630 Hz, 60 km/h)	81@60 km/h;	/
	60		80@(500 Hz, 100 km/h)	84@100 km/h	
	100	M4	78@(630 Hz, 60 km/h)	79@60 km/h;	/
			76@(630 Hz, 100 km/h)	82@100 km/h	
		M9	73@(630 Hz, 60 km/h)	76@60 km/h;	/
			73@(630 Hz, 100 km/h)	79@(100 km/h)	
		M12	68@(630 Hz, 60 km/h)	72@60 km/h;	/
			71@(630 Hz, 100 km/h)	75@100 km/h	
		MB1	79@(80 Hz, 40 km/h)	85@40 km/h	/
			83@(50 Hz, 60 km/h)	88@ 60 km/h	
		MB2	74@(63 Hz, 40 km/h)	80@40 km/h	/
			80@(31 Hz, 60 km/h)	85@ 60 km/h	
		VB1	102@(50 Hz, 40 km/h)	106@40 km/h	/
			106@(40 Hz, 60 km/h)	111@60 km/h	
		VB2	99@(63 Hz, 40 km/h)	102@40 km/h	/
			103@(31 Hz, 60 km/h)	107@60 km/h	
Straight barrier	100	M1	65@630 Hz	70	14
		M4	73@630 Hz	78	4
		M9	65@630 Hz	70	9
		M12	64@630 Hz	70	5
Semi-closed barrier	60	M1	67@1000 Hz	70	11
		M4	68@1000 Hz	72	7
		M9	57@1000 Hz	62	14
		M12	61@1000 Hz	66	6
Rubber floating slab track	40	M1	81@(800 Hz, 40 km/h)	83@40 km/h	/
	60		81@(800 Hz, 60 km/h)	84@60 km/h	
		M4	81@(800 Hz, 40 km/h)	84@40 km/h	/
			82@(800 Hz, 60 km/h)	86@60 km/h	
		M9	70@(800 Hz, 40 km/h)	73@40 km/h	/
			71@(630 Hz, 60 km/h)	75@60 km/h	
		M12	71@(800 Hz, 40 km/h)	75@40 km/h;	/
			72@(800 Hz, 60 km/h)	77@60 km/h	
		MB1	79@(50 Hz, 40 km/h)	83@ 40 km/h	2@40 km/h
			80@(50 Hz, 60 km/h)	84@ 60 km/h	4@60 km/h
		MB2	75@(63 Hz, 40 km/h)	80@ 40 km/h	0@40 km/h
			75@(63 Hz, 60 km/h)	82@ 60 km/h	3@60 km/h
		VB1	104@(63 Hz, 40 km/h)	105@40 km/h	1@40 km/h
			104@(63 Hz, 60 km/h)	106@60 km/h	5@60 km/h
		VB2	93@(50 Hz, 40 km/h)	99@40 km/h	3@40 km/h
			97@(31 Hz, 60 km/h)	102@60 km/h	5@60 km/h
Track acoustic absorber	40	M1	70@(1250 Hz, 40 km/h)	78@40 km/h	5@40 km/h
	60		75@(630 Hz, 60 km/h)	81@60 km/h	3@60 km/h
		M4	73@(800 Hz, 40 km/h)	79@40 km/h	5@40 km/h
			78@(800 Hz, 60 km/h)	83@60 km/h	3@60 km/h
Track-side barrier	40	M1	63@(500 Hz, 40 km/h)	69@40 km/h	14@40 km/h
	60		72@(800 Hz, 60 km/h)	74@60 km/h	10@60 km/h
		M4	67@(500 Hz, 40 km/h)	71@40 km/h	13@40 km/h
			75@(800 Hz, 60 km/h)	77@60 km/h	9@60 km/h
		M9	58@(800 Hz, 40 km/h)	62@40 km/h	11@40 km/h
			65@(800 Hz, 60 km/h)	68@60 km/h	7@60 km/h
		M12	54@(800 Hz, 40 km/h)	59@40 km/h	16@40 km/h
			62@(800 Hz, 60 km/h)	66@70 km/h	11@60 km/h
Acoustic absorber combined with track-side barrier	40	M1	57@(500 Hz, 40 km/h)	62@40 km/h	21@40 km/h
	60		65@(800 Hz, 60 km/h)	70@60 km/h	14@60 km/h
		M4	66@(800 Hz, 40 km/h)	68@40 km/h	16@40 km/h
			76@(800 Hz, 60 km/h)	72@60 km/h	13@60 km/h
		M9	52@(800 Hz, 40 km/h)	57@40 km/h	16@40 km/h
			60@(800 Hz, 60 km/h)	64@60 km/h	10@60 km/h
		M12	54@(800 Hz, 40 km/h)	59@40 km/h	16@40 km/h
			64@(800 Hz, 60 km/h)	67@60 km/h	9@60 km/h

km/h, insertion losses for all measuring points were above 10 dB(A); and at 60 km/h, the insertion losses reduce slightly, where at least 7 dB(A) is achieved. The three kinds of noise barriers are found to have similar performance at the lowest measuring point (M1), even though this point has exceeded the height of track-side barrier. The track-side barrier shows a larger efficient noise mitigation region than the straight barrier for near field locations and is competitive with the semi-closed barrier when the noise reception height is below 7.5 m from the track plane. Measurement results in the case of simultaneous deployment of track-side noise barrier and track acoustic absorber is shown in Fig. 10. The combined effect is quite positive. An insertion loss of 21 dB(A) is found at the point M1 under 40 km/h. Around 2–7 dB(A) boosts on insertion losses are found at different measuring points by comparison with the solely track-side noise barrier scenario. An improvement in mitigation

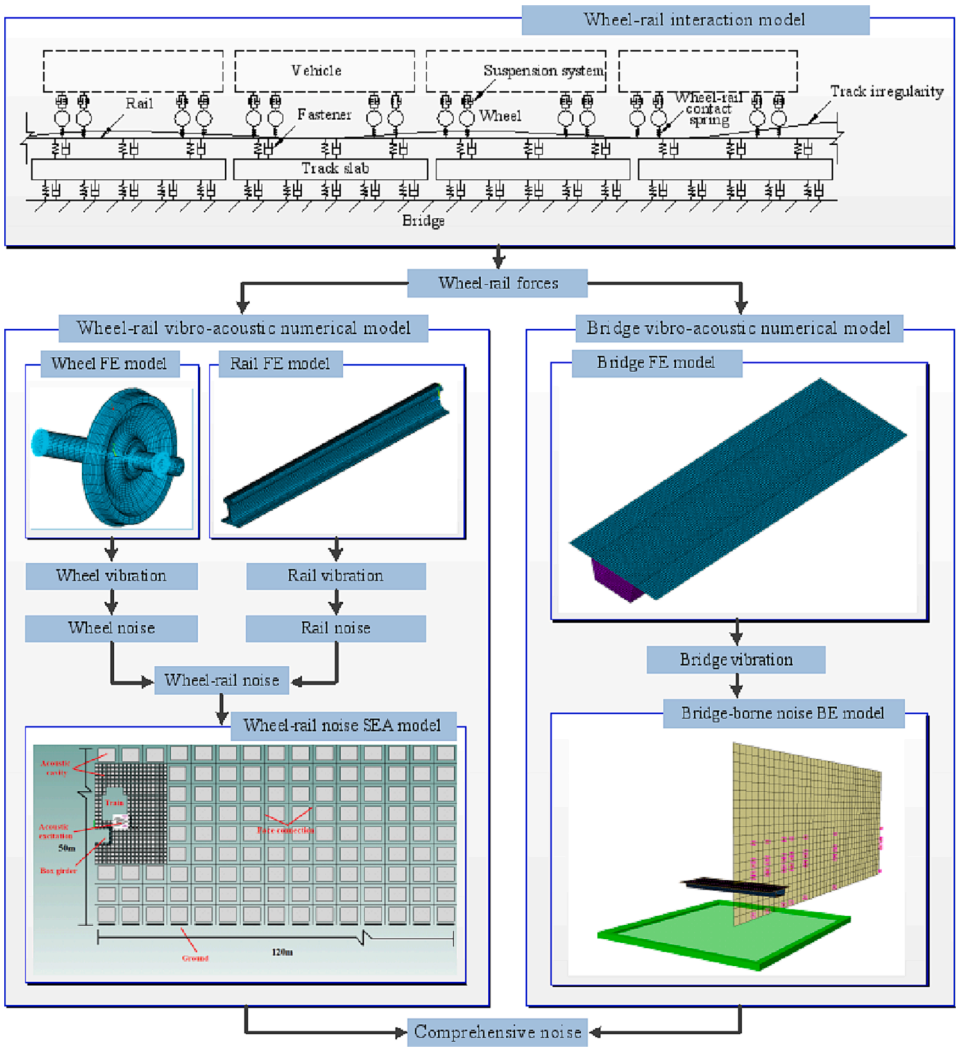

Fig. 11. Numerical simulation procedures of train-induced noise.

Table 3
Model parameters of the train, rail, and bridge.

Component	Parameter	Unit	Value
Train	Mass of bogie	t	2.43
	Mass of wheelset	t	1.744
	Stiffness of primary suspension	kN/m	1252
	Length between bogie centers	mm	15,700
	Wheelbase	mm	2500
	Wheel diameter	mm	860
	Wheel density	kg/m^3	7850
	Young's modulus of wheel	N/m^2	2.06×10^{11}
	Poisson's ratio of wheel	/	0.3
	Loss factor of wheel	/	0.0001
Rail	Cross-section area of rail	mm^2	7745
	Rail density	kg/m^3	7850
	Young's modulus of rail	N/m^2	2.06×10^{11}
	Poisson's ratio of rail	/	0.3
	Loss factor of rail	/	0.01
	Fastener stiffness	MN/m	60
	Fastener spacing	m	0.625
Bridge	Height of box-girder	m	2.15
	Width of bridge deck	m	10.9
	Width of bridge bottom	m	5.4
	Bridge density	kg/m^3	2420
	Young's modulus of bridge	N/m^2	3.45×10^{10}
	Poisson's ratio of bridge	/	0.2
	Loss factor of bridge	/	0.02

efficiency from the combined strategy is observed.

Measurements supporting the above discussions are summarized in Table 2. Several preliminary speculations and questions are raised for further discussions:

- Intuitively, semi-closed barrier used for elevated railway is supposed to have a better noise mitigation efficiency for nearby high-rise buildings than straight barrier and track-side barrier, but the measurement results do not coincide with this intuition. Are there any situations where the semi-closed barrier can outperform the other two types?
- The measurement results in the case of track acoustic absorber show a uniform noise mitigation performance from all the measuring points. However, a full picture describing how track acoustic absorber hinders the noise radiation at larger distances is expected.
- The track-side noise barrier seems to have a larger efficient noise reduction region than the straight noise barrier does. Thus the following question arises: Does the track-side barrier outperform the straight noise barrier in general?

In the next section, a numerical model will be developed with an attempt to address the above issues, and the numerical results will be used to interpret the noise reduction characteristics of the control strategies studied above. Furthermore, the numerical model, after calibrated

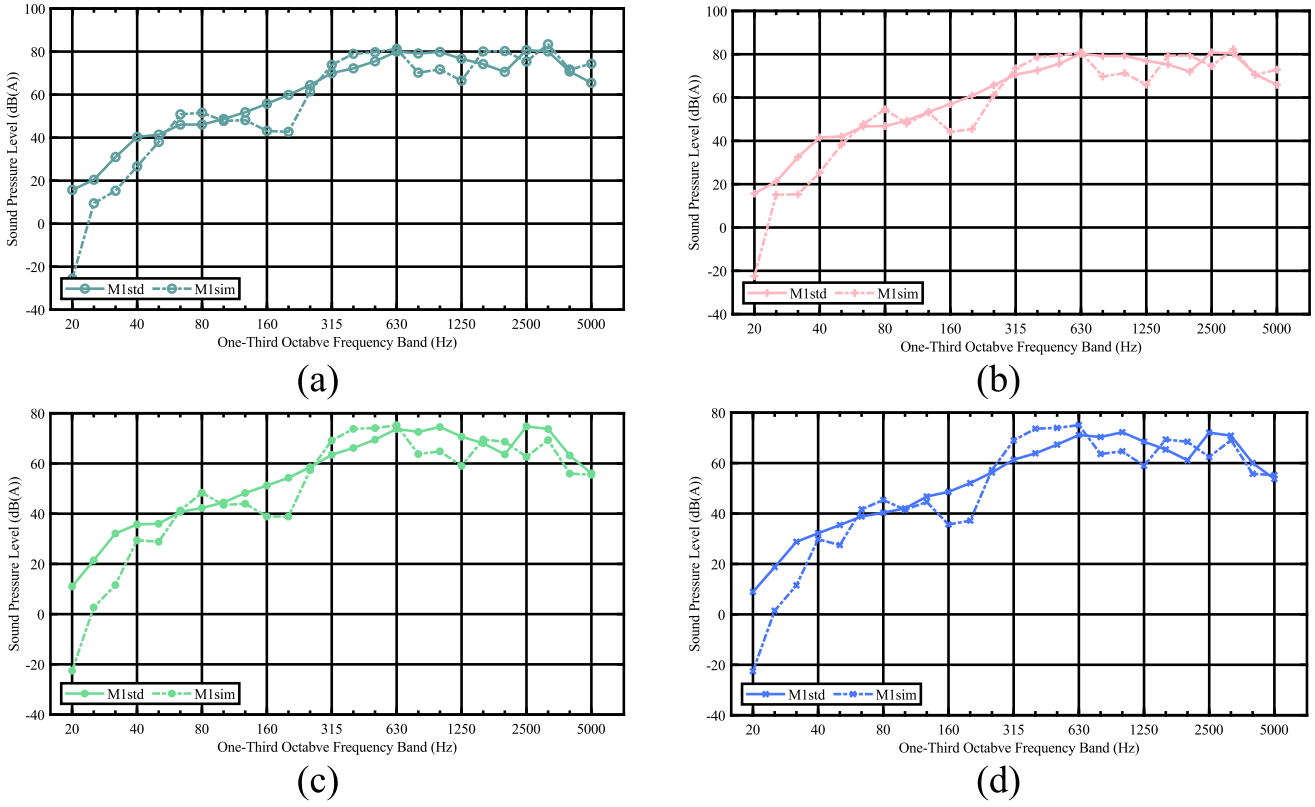

Fig. 12. Model calibration based on measurements from standard section at 94 km/h: (a) M1; (b) M2; (c) M9; (d) M10 (std: standard section; sim: simulated result).

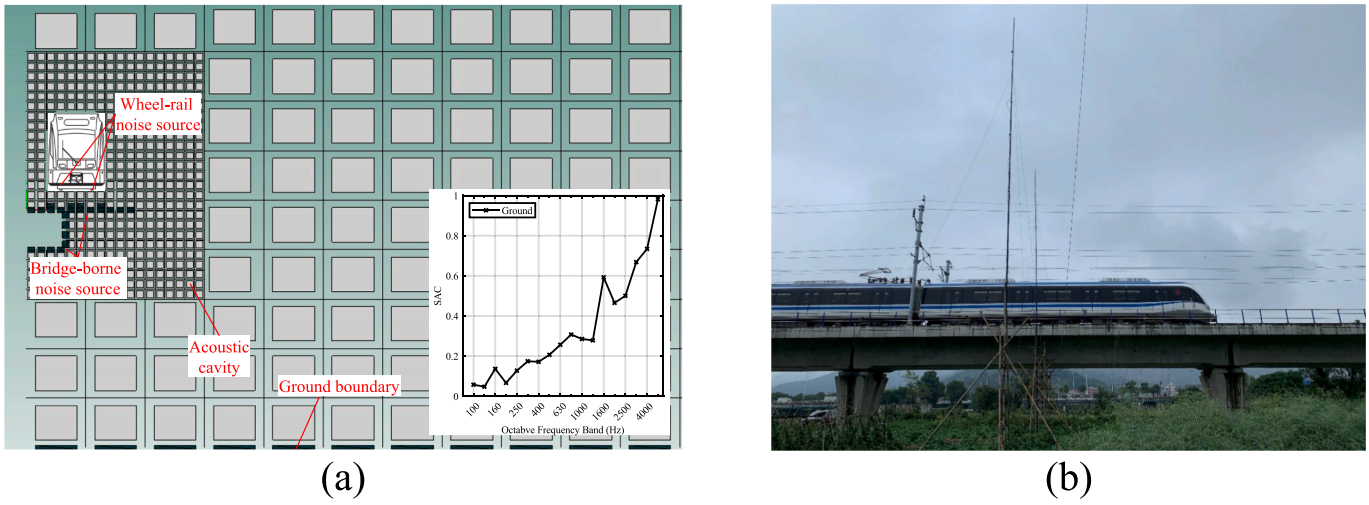

Fig. 13. Standard section as a baseline: (a) modelling setup and sound absorption coefficient (SAC) spectrum of ground; (b) site condition.

with in-situ measurement data, will provide a reference that could help answer the following question important in practice: what kind of noise mitigation measure shall be used for a specific elevated suburban railway?

3. Numerical model

In the model developed for this study, wheel-rail rolling noise and bridge-borne noise are considered as the predominant noise sources of the elevated suburban rail. The track irregularities have been concluded as the primary excitation for these two kinds of noise sources [5,21,42,43]. Therefore, a superposition procedure is employed to calculate the combined train-induced noise, as shown in Fig. 11. Wheel-rail rolling noise is simulated through an SEA model with the interaction force spectrum as system inputs. The structure-borne noise, including the bridge-borne noise and barrier-borne noise, is calculated through a BEM model with the same interaction force spectrum. The train-track interaction model takes the rail irregularities as input to generate the force spectrum. At last, the calculated wheel-rail noise and structure-borne noise are summed together as the overall train-induced noise output.

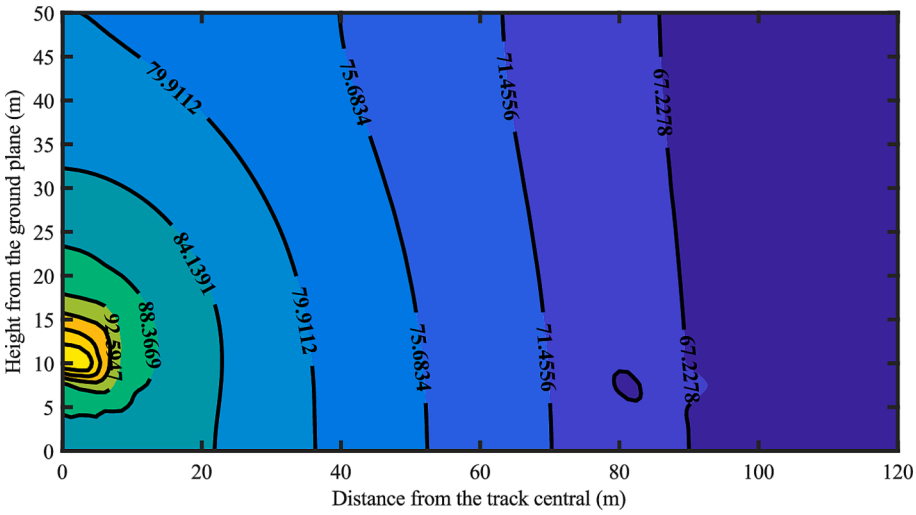

Fig. 14. Noise distribution map of standard section.

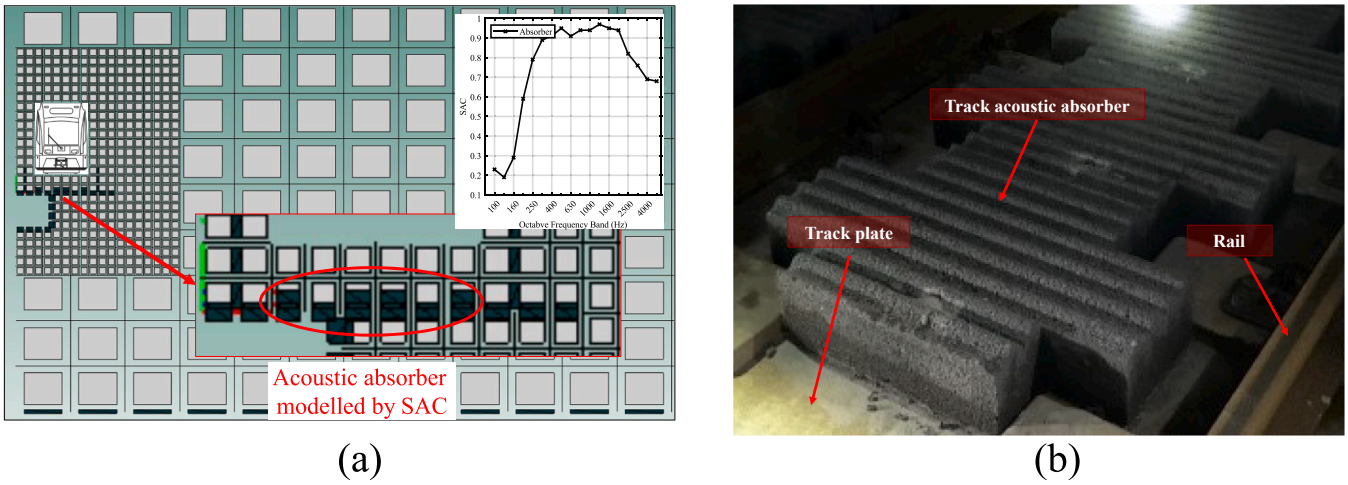

Fig. 15. Track acoustic absorber: (a) modelling setup and sound absorption coefficient of absorber (SAC); (b) site condition.

3.1. Model development

3.1.1. Train-track interaction model

Although extensive investigations have been carried out on developing advanced train-track rolling contact models [44–48], the effectiveness of basic Hertz contact theory has been well demonstrated in predicting the steady-state wheel-rail rolling noise [42,49–51]. As a result, the train-track interaction model based on the dynamic receptance method [42] takes the rail roughness, wheel, rail and contact receptance as model inputs

$$F(\omega) = \frac{R(\omega)}{A_w + A_R + A_C} \tag{1}$$

where $R(\omega)$ denotes rail roughnesses, A_w, A_R and A_C are the receptances of wheel, rail and contact spring. Rail roughnesses refer to the ISO 3095 (2005) standard [52], holding a relation with the irregularity wavelength, written as [53]

$$20\log\left(\frac{R}{r_0}\right) = \begin{cases} 18.45\log(\lambda) + 27.0 = 20 & \lambda > 0.01\ m \\ -9.70 & \lambda < 0.01\ m \end{cases} \tag{2}$$

where r_0 is the reference rail roughness whose value is 10^{-6} m, and λ is the wavelength of the rail roughness. The relevant model parameters are listed in Table 3.

3.1.2. Wheel-rail rolling noise prediction model

Finite element (FE) models of wheel and rail are established with the commercial software ANSYS to obtain the interaction-induced vibration of both wheel and rail. The obtained vibration will later be input to a vibroacoustic software (VA one, statistical energy analysis) for noise radiation analysis.

Eight-node solid element is utilized to formulate both wheel and rail FE models. A total of 11,260 elements with mesh size no more than 0.0675 m are generated for the wheel. The rail is meshed along its cross-section and then extruded along the longitudinal direction. 132 elements with 0.01 m mesh size are generated for the planar cross-section. The longitudinal extruding also adopts the 0.01 m mesh size.

In the SEA model, simulated wheel and rail vibration responses are transferred as acoustic boundary condition and then input into the SEA model to calculate the noise radiation. The noise absorption and reflection of ground, bridge and sound barrier are considered, thus being capable of capturing the noise radiation pattern of different noise barriers. The noise insulation effect of train body is also considered by eliminating the acoustic cavity in the train operating region.

3.1.3. Bridge-borne noise model

The bridge structure is established as an FE model to obtain the vibration response under the train-track interaction force. Considering the inefficiency of SEA in acoustic radiation analysis for lower frequency

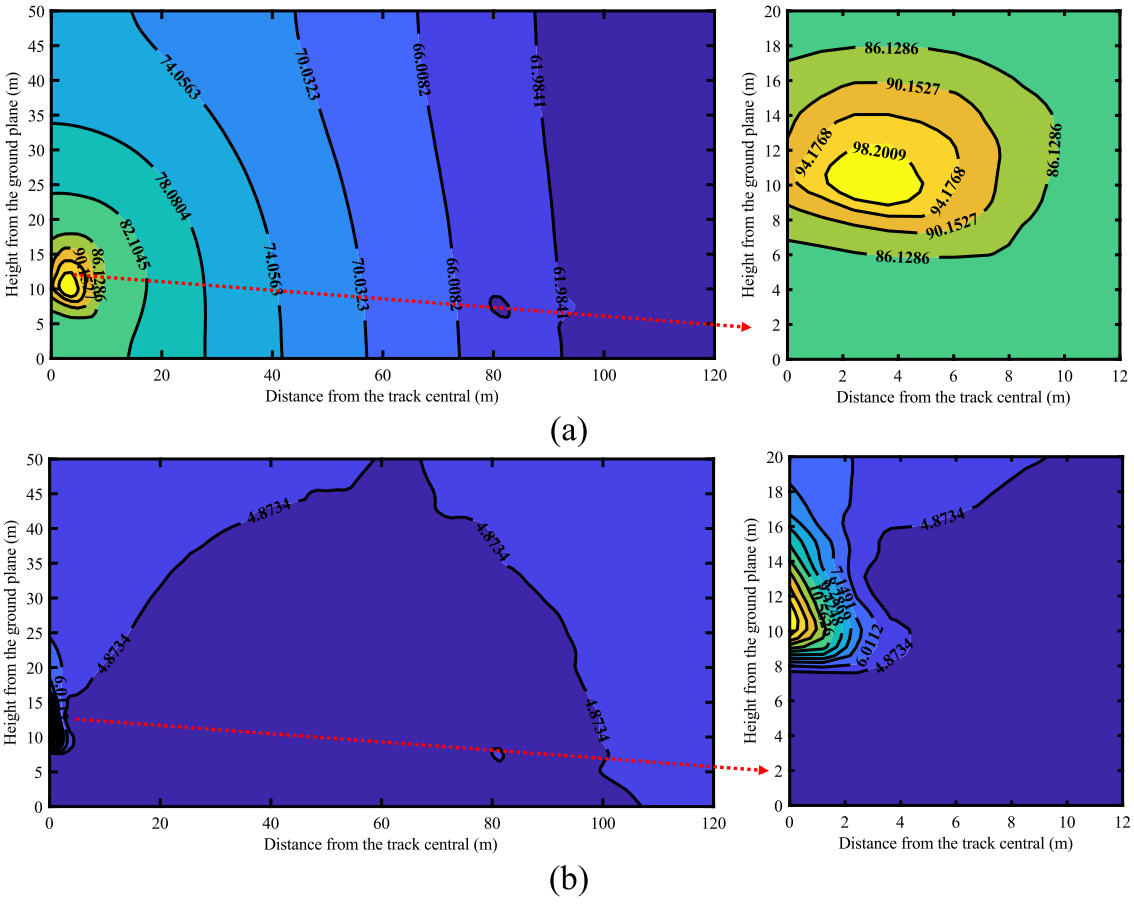

Fig. 16. Simulation results of track acoustic absorber: (a) noise distribution map, and (b) insertion loss map.

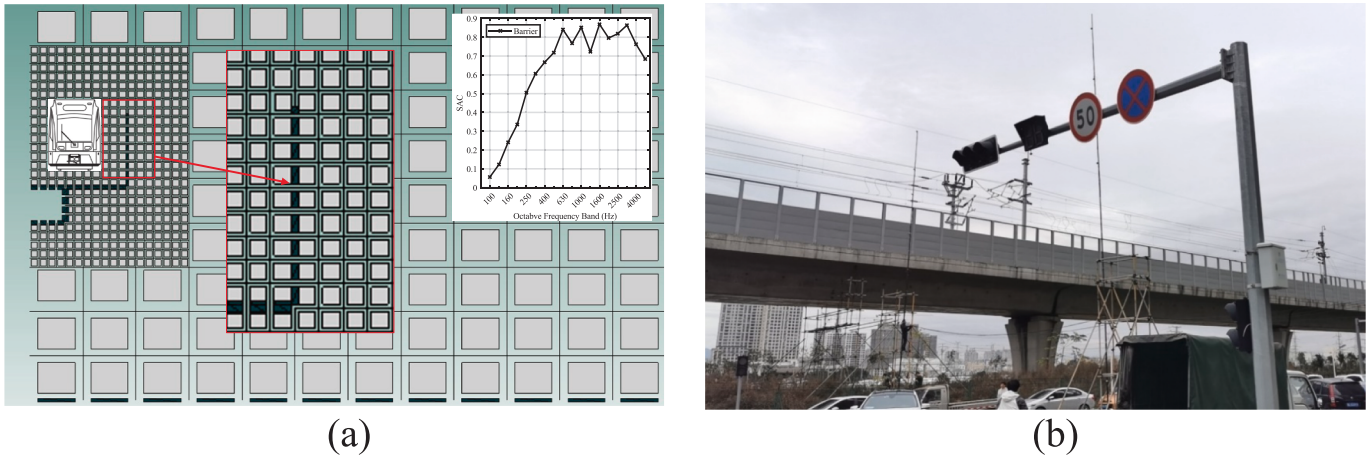

Fig. 17. Straight noise barrier: (a) modelling setup and sound absorption coefficient (SAC); (b) site condition.

components, BEM is utilized for acoustic radiation analysis based on the generated vibration response. Four-node shell elements are used to model the box girder with a mesh size no more than 0.25 m, and a total of 12,900 elements are generated.

3.1.4. Overall noise

The overall noise is obtained through a superposition of wheel-rail noise and bridge-borne noise. The sound energy of wheel-rail noise is mainly concentrated in medium- and high-frequency bands of 500 to 2000 Hz [5,42] while the sound energy of bridge-borne noise is mainly concentrated in the low-frequency band below 200 Hz [11,27,54,55]. Therefore, taking 200 Hz as a boundary, the wheel-rail noise model is used to predict the noise in the frequency band of 200 to 5000 Hz; meanwhile, the bridge-borne noise is used to predict the noise in the frequency band below 200 Hz [56].

3.2. Model calibration

The numerical model is calibrated with measurement data from the standard section. Measurements with a train speed of 94 km/h, which is the median value among the measured three repetitive runs under the 100 km/h nominal speed, are utilized. Four measuring points (M1, M2,

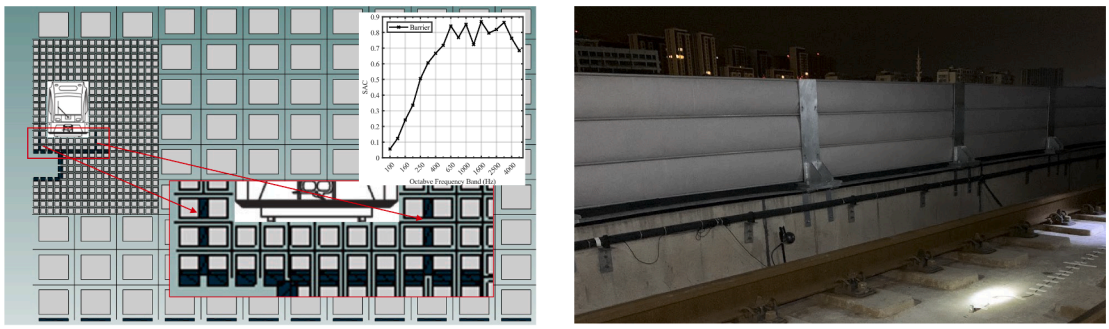

Fig. 18. Track-side noise barrier: (a) modelling setup and sound absorption coefficient (SAC); (b) site condition.

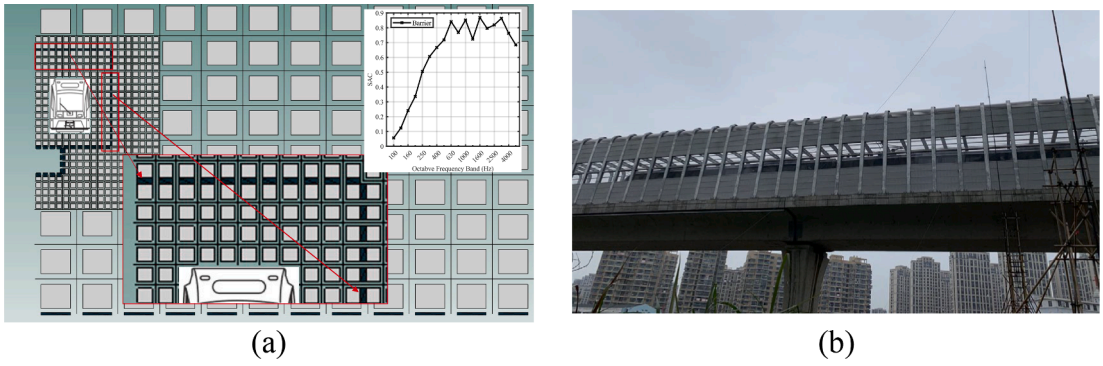

Fig. 19. Semi-closed noise barrier: (a) modelling setup and sound absorption coefficient (SAC); (b) site condition.

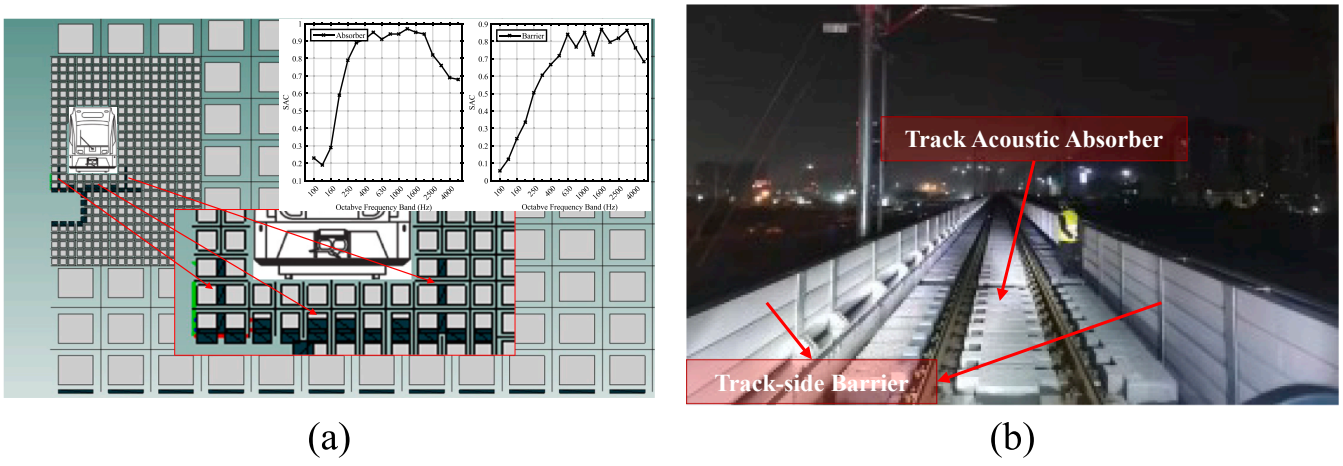

Fig. 20. Track-side noise barrier combined with track acoustic absorber: (a) modelling setup and sound absorption coefficient (SAC); (b) site condition.

M9, M10) are chosen for the calibration in line with the measuring locations recommended in relevant standard [52]. Recall that the proposed model is to evaluate the efficiency of various noise mitigation measures, and therefore, it is crucial to calibrate the numerical model to the baseline measurement, ensuring its prediction capability in terms of both the amplitudes of sound pressure level and the corresponding spectrum characteristics. Fig. 12 presents the calibration results, a satisfactory agreement is achieved in terms of both SPL amplitudes and spectrum characteristics. Based on the calibrated baseline model, the noise mitigation measures will be incorporated in the calibrated model, with the same speed, aiming to provide information with the intent of explaining the findings from measurements and to determine preferred noise mitigation strategies by considering both mitigation efficiency and cost-effectiveness.

4. Numerical interpretation and discussion

The noise mitigation measures presented in section 2 are simulated by the calibrated model to figure out the noise mitigation features of track acoustic absorber, and the efficient noise reduction regions of straight barrier, track-side barrier, and semi-closed barrier. Their performance margins will be compared based on the relative percentage of insertion losses (taking the location of the measuring point M1 as a baseline value), and the efficient noise reduction regions versus different barrier types will be obtained. With the comparative experimental evaluation and numerical interpretation, recommendations on the

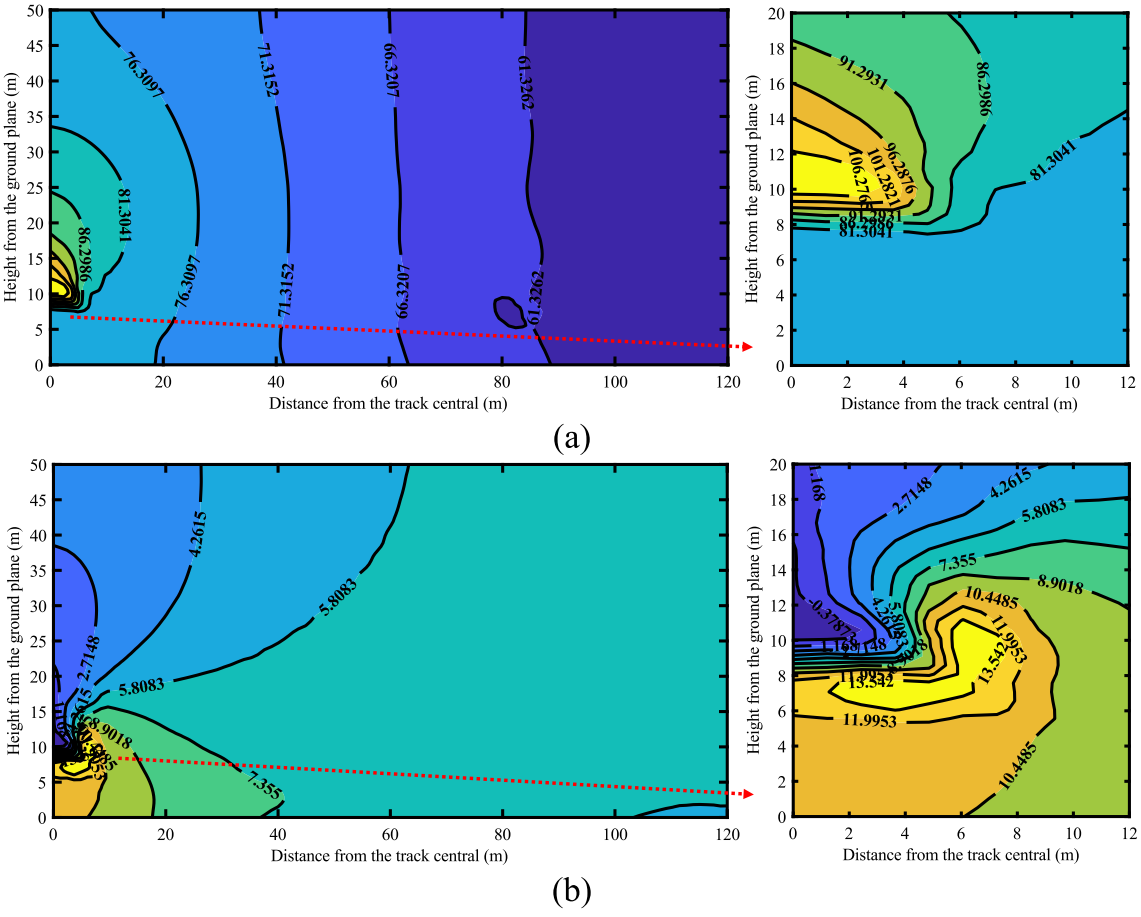

Fig. 21. Simulation results of straight barrier: (a) noise distribution map, and (b) insertion loss ma.

choice of barrier types will be provided at the end of this section.

Fig. 13 shows the modelling setup of the standard section and the corresponding measurement site condition. The sound reflection effects of both bridge and ground are taken into account. The sound absorption coefficient of ground is determined by measurement [57].

Fig. 14 illustrates the spatial distribution of noise for the standard section. The discussions below will be based on this baseline contour map. The spatial region holds a lateral distance range from 0 and 120 m to the track central line and a vertical distance range between 0 and 50 m to the ground. The bridge bottom plate and track plane are set as 10 m and 12.5 m away from the ground level, respectively. This 120 m $\times$ 50 m spatial region is large enough to cover most of the concerned spaces in relation to railway noise mitigation.

4.1. Noise reduction feature of track acoustic absorber

The track acoustic absorber (Fig. 15) is modelled by adjusted sound absorption coefficient (SAC) around the track region. The SAC of track acoustic absorber is obtained through a series of laboratory experiments, and the obtained spectrum is plotted inside Fig. 15(a).

Fig. 16 shows the noise distribution map and noise reduction map of track acoustic absorber. In comparison with the simulation results of the standard section (Fig. 14), it is found that the track acoustic absorber does not change the noise radiation feature. Its noise mitigation efficiency map is also uniformly distributed along with both the vertical and lateral distances. The simulation results agree favorably with the field observation, concluding that the track acoustic absorber holds uniform noise mitigation efficiency when the noise reception point is more than 7.5 m away from the track central line. At the measuring point M1, the track acoustic absorber possesses an insertion loss of 4.4 dB(A).

4.2. Efficient noise reduction regions

The modelling setup for straight noise barrier, track-side noise barrier, semi-closed noise barrier, and track-side noise barrier in combination with track acoustic absorber are presented in Figs. 17–20. The straight barrier and semi-closed noise barrier are installed 3.2 m away from the nearest track center, while the distance for the track-side noise barrier reduces to 1.9 m. The acoustic insulation performance of noise barrier is also simulated with SAC that was measured through laboratory experiments, and the SAC spectra are plotted inside the corresponding modelling setup figures.

The noise distribution map, insertion loss map, and ratio of insertion loss for the three types of noise barriers are presented in Figs. 21–23. To describe the spatial deterioration of insertion loss of different noise mitigation strategies, the insertion loss at measuring point M1 is used as a baseline insertion loss (baseline performance) for further comparison. In Fig. 21(b), the largest insertion loss of straight barrier is found at locations between 2 m and 8 m laterally away from the track central line, and below the track plane (12.5 m). The height of straight barrier is 3.5 m, and thus this barrier structure ranges from 12.5 m to 16 m vertically. The insertion loss decreases rapidly with height, and can only achieve 50% of its performance when the reception point is higher than 14 m and near the barrier, indicating that the straight barrier is not efficient in mitigating noise for nearby and high reception points. Having said that, this kind of decrease slows down with increasing lateral distance. The straight barrier is found to have at least 60% of its baseline performance for the reception point that is more than 40 m laterally away from the track center. Practically speaking, straight noise barrier is less effective for buildings that are higher than 20 m and are located within 20 m laterally away from the track central line. In other words, it is

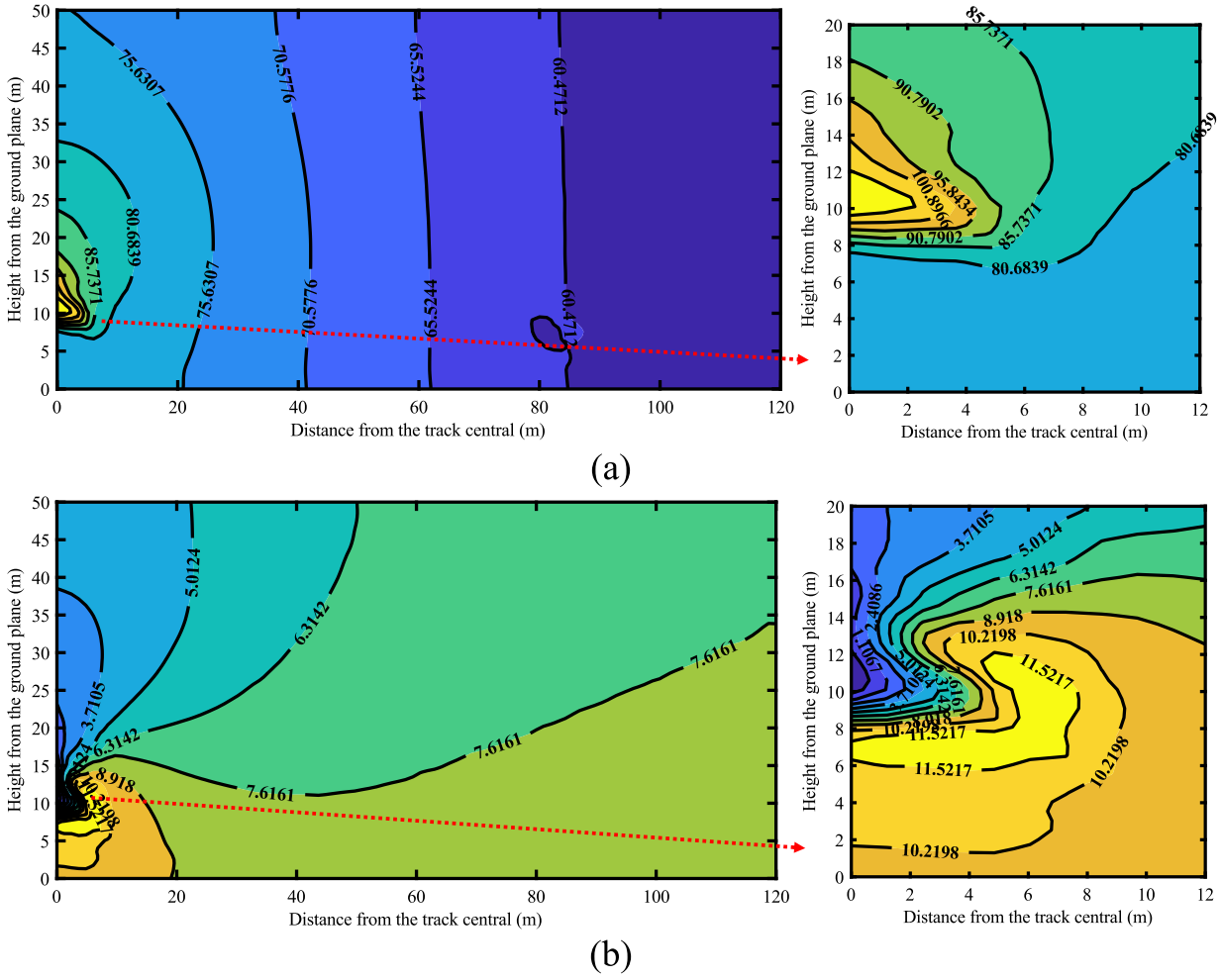

Fig. 22. Simulation results of track-side barrier: (a) noise distribution map, and (b) insertion loss map.

inappropriate to choose the straight barrier as a potential noise mitigation measure to neighboring high-rise buildings.

The track-side barrier holds very similar noise mitigation features as the straight barrier does (Fig. 22(b)). Slightly better performance than the straight barrier is found in the far-field point that is more than 40 m laterally away from the track central line. The insertion loss of the track-side barrier is still rapidly decreasing with lifting reception point, showing its noise reduction inefficiency when applied for nearby high-rise buildings. Nevertheless, considering its very limited structure height (0.94 m) and slightly better performance than the straight barrier (especially for far-field points), the track-side noise barrier is a good alternative to the straight noise barrier because of achieving identical performance while saving construction material.

The semi-closed noise barrier, in general, is one of the most effective noise mitigation measures among all railway noise control measures. In the numerical model, the semi-closed noise barrier is found to be much more efficient than the other two kinds of barriers. In Fig. 23(b), at the baseline point (M1), the insertion loss can reach about 20 dB(A), and the insertion loss does not rapidly deteriorate with the increasing height once the measuring point is 4 m away from the track center. The semi-closed barrier is found to have at least 70% of its baseline performance in nearly the whole simulation field. The above numerical results indicate appealing noise reduction performance from the semi-closed noise barrier, which, however, does not coincide with the in-situ measurements. Such numerical overestimation can be attributed to the perfect sealing condition in the numerical model, which will inevitably deteriorate over time in engineering practice [58]. The randomly distributed gaps or apertures on the noise barrier cannot be reasonably modelled by the current numerical techniques. As a result, the numerical model generates different results from in-situ measurements, and the actual performance of semi-closed noise barrier seems to be more related to the barrier integrity and site conditions instead of the structure characteristic itself.

Fig. 24(b) shows the combined effect of track acoustic absorber and track-side barrier. In comparison with Fig. 22(b), approximately 3–5 dB (A) boost on the insertion loss is achieved by this combined strategy, which agrees well with the measurements. This combined control strategy essentially makes the benefit of two kinds of separate mitigation measures without sacrificing their individual performance. The obtained insertion loss is basically identical to the linear sum of two separate measures. This strategy shows a better noise mitigation efficiency in nearby and high regions than the track-side noise barrier alone, and, according to the measurement results, it will be practically more efficient than the semi-closed noise barrier for noise mitigation even at the locations below the height of 20 m and within 20 m laterally away from the track central line.

Fig. 25 summarizes the insertion losses at measuring point M1 based on both experimental measurements and simulation results. Although the train speed considered in the numerical model is somehow different from the measurements, the predictions overall capture the trends of various noise mitigation strategies, except for the semi-closed barrier. As a result, these simulated noise distribution maps and insertion loss maps presented in this subsection, especially the far-field predictions, can partially compensate for the limitations of in-situ experimental

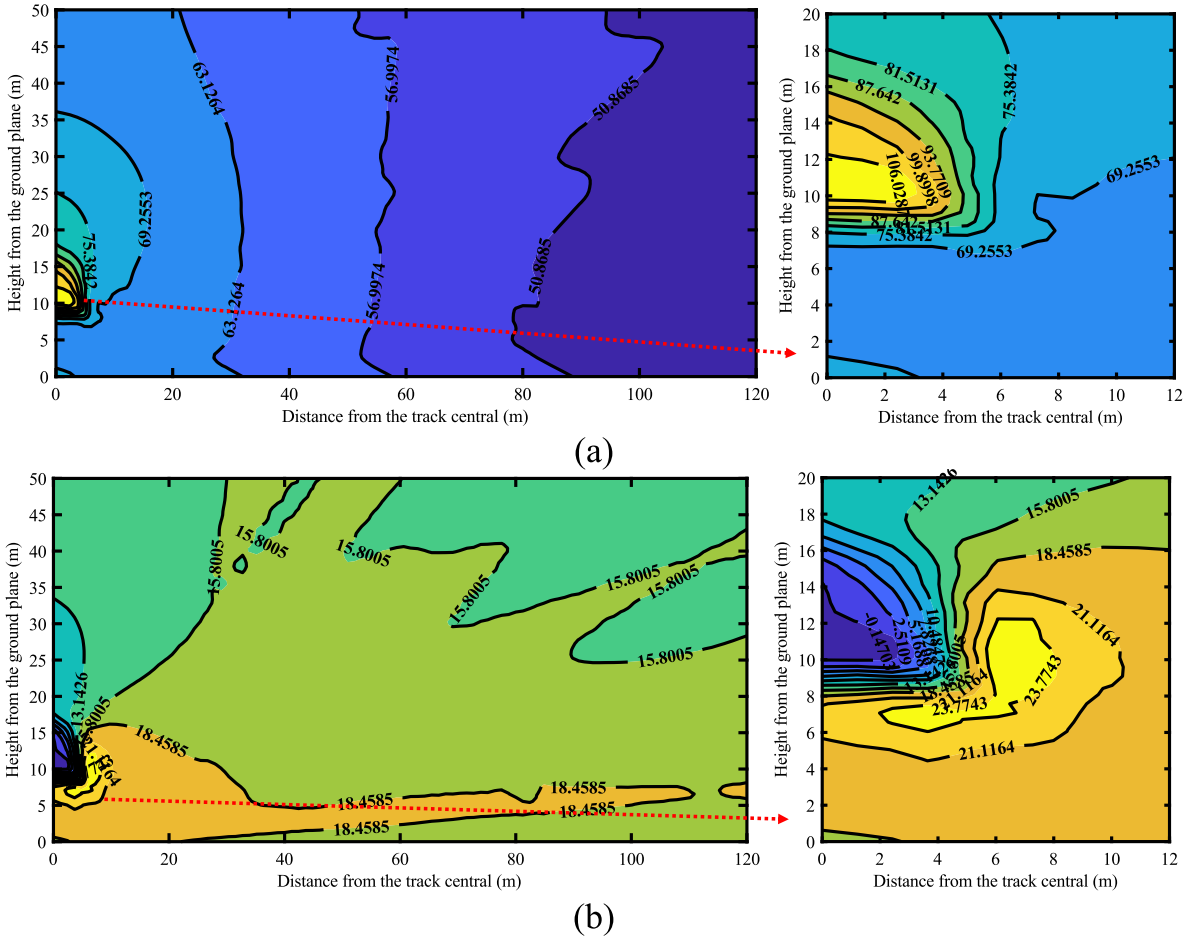

Fig. 23. Simulation results of semi-closed barrier: (a) noise distribution map, and (b) insertion loss map.

evaluations and offer valuable insights for parties concerned with radiated far-field noise.

The above numerical simulation results can help to answer the questions raised in section 2.2:

- The numerical models show that semi-closed noise barrier has a much greater performance than straight noise barrier and track-side noise barrier for all measuring points, which however is contradictory to the in-situ measurements. Comprehensively considering the numerical and measurement results, the well-maintained semi-closed noise barrier can outperform the other two types of noise barrier in their rapidly deteriorating region, which is about 2.5 m above the track plane and within the 20 m away from the track center. Once these areas become noise sensitive, a semi-closed noise barrier should be applied, and careful maintenance after implementation is necessary;
- Track acoustic absorber shows consistent noise mitigation efficiency for all measuring points, and the numerical modelling results coincide well with the measurements. Track acoustic absorber is demonstrated to be a good supplementary noise mitigation measure that can be adopted in a combined noise control strategy;
- Track-side noise barrier and straight noise barrier hold nearly the same spatial distribution characteristics on their insertion losses, and the former shows overall better performance and should be more widely applied. Taking 60% of reduction efficiency as an indicator of ineffective region, Fig. 21, Fig. 22 and Fig. 24 clearly show the margins, and a combined track acoustic absorber and track-side noise barrier can effectively improve the efficient noise reduction region.

The above investigations have revealed the characteristics of various noise mitigation measures considered, which can be directly referred to when making decisions on selection/implementation of noise control measures for similar rail transit structures. As regards the question "what kind of noise mitigation measure shall be used?" raised before, the recommendation is that, for buildings with heights above 20 m and approximately 20 m away from the track center, the well-maintained semi-closed noise barrier is the only available option that could provide higher insertion losses. Otherwise, combining track-side noise barrier and track acoustic absorber will be the most suitable combined noise control strategy, which simultaneously ensures cost-effectiveness and noise mitigation efficiency. Besides, without using the track acoustic absorber, the track-side barrier can slightly outperform the straight barrier, which therefore should be more widely applied in engineering practice.

5. Conclusions

Experimental evaluation of a series of noise and vibration mitigation strategies was conducted in this study. Numerical interpretation on top of the experimental evaluation was then presented to further illustrate the noise reduction features of different control strategies. The results obtained from the combined investigation of measurements and numerical modelling can serve as a guide for selecting appropriate noise control strategies in engineering practice. Major findings of this study are summarized as follows:

1. Rubber floating slab track is experimentally found to be effective in mitigating the bridge vibration and the corresponding bridge-borne

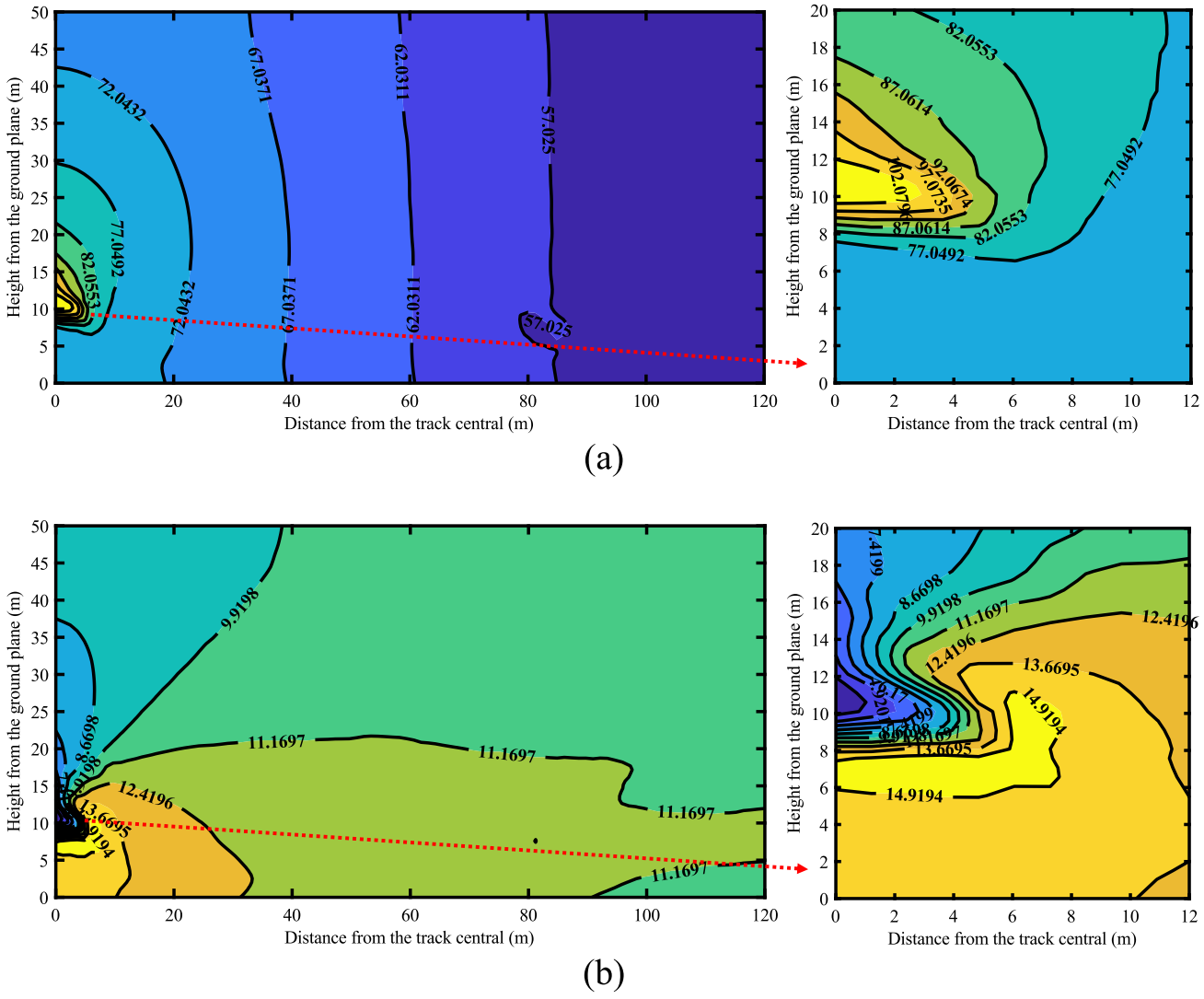

Fig. 24. Simulation results of track acoustic absorber combined with track-side noise barrier: (a) noise distribution map, and (b) insertion loss map.

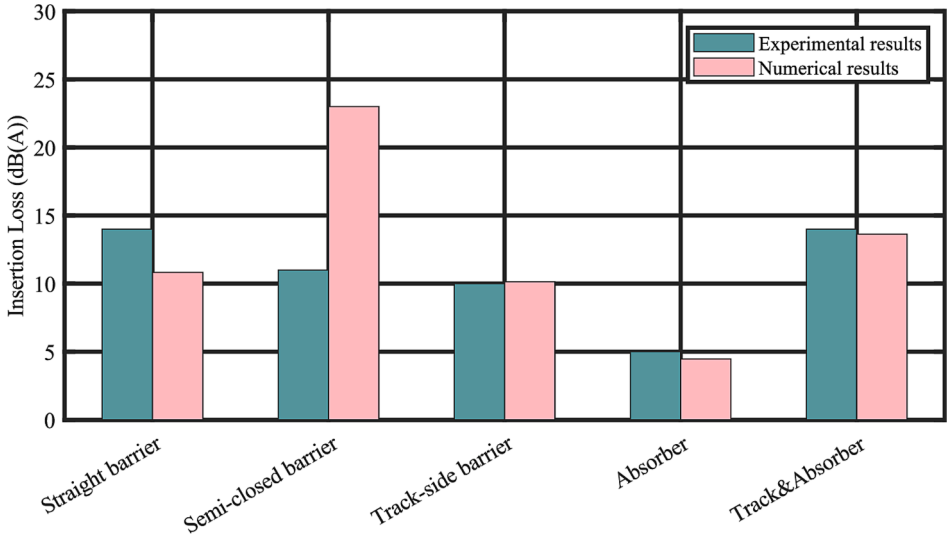

Fig. 25. A summary of insertion losses at measuring points M1. Numerical results at 94 km/h versus experimental results at their highest available speeds (correspond to Table 2).

noise by 1–5 dB VAL and 0–4 dB(L) SPL. It is more efficient when the train is travelling in a higher speed. This mitigation measure should be utilized jointly with other measures when both bridge-borne noise and bridge vibration are concerned;
2. Track-side noise barrier and straight noise barrier hold very similar performance. Their insertion losses deteriorate rapidly in the neighboring and high regions; and therefore, both kinds of noise barriers should not be adopted when the noise sensitivity region is at their worst performance region, which is within 20 m away from the track center and 2.5 m above the track plane;
3. Track acoustic absorber is a good supplementary measure that provides noise reduction for all measuring points. A combined application of track-side noise barrier and track acoustic absorber can achieve a boost on insertion loss for 2–5 dB(A). It can also effectively improve the efficient noise reduction region;
4. Semi-closed noise barrier is numerically and intuitively the most efficient measure in train-induced noise reduction, but its performance will be diminished by the deteriorated sealing performance. Timely maintenance is necessary to keep a good performance of semi-closed noise barrier. It should be applied only for noise mitigation of nearby regions (<20 m from the track center) and high-rise buildings (greater than 2.5 m from the track plane).

In this paper, the main conflict is found between the numerical and experimental results in the case of semi-closed noise barrier. The discrepancy is attributed to the structural sealing deterioration [18] that can be induced by train-induced vibration and airflows [59–61]. A monitoring strategy detecting the sealing status of semi-closed noise barrier is thus demanding. Also, a more powerful modelling technique taking into account the sealing deterioration is expected. It is worth mentioning that the conclusions drawn for various mitigation measures in this study are adaptive to cases where the wheel-rail rolling noise is predominant.

CRediT authorship contribution statement

Yun-Ke Luo: Methodology, Data curation, Software, Writing – original draft, Visualization. **Li-Zhong Song:** Methodology, Formal analysis, Validation. **Chao Zhang:** Data curation, Visualization. **Yi-Qing Ni:** Conceptualization, Resources, Writing – review & editing, Supervision, Project administration, Funding acquisition.

Declaration of Competing Interest

The authors declare that they have no known competing financial interests or personal relationships that could have appeared to influence the work reported in this paper.

Data availability

Data will be made available on request.

Acknowledgments

The work described in this paper was supported by the Innovation and Technology Fund (ITF) (Grant No. ITS/096/21) from the Innovation and Technology Commission (ITC) of the Hong Kong Special Administrative Region, China. The authors would also like to appreciate the funding support by ITC to the Hong Kong Branch of Chinese National Rail Transit Electrification and Automation Engineering Technology Research Center (Grant No. K-BBY1), the National Natural Science Foundation of China (Grants No. U1934209 and 52008169), and the Open Fund of State Key Laboratory of Performance Monitoring and Protecting of Rail Transit Infrastructure, East China Jiaotong University, Nanchang, China (Grant No. HJGZ2021108).

References

[1] B. Flyvbjerg, N. Bruzelius, B. van Wee, Comparison of capital costs per route-kilometre in urban rail, Eur. J. Transp. Infrastruct. Res. 8 (2008) 17–30.
[2] A.K. Gorai, A.K. Pai, Noise and its effect on human being-a review, J. Environ. Sci. Eng. 48 (2006) 253–260.
[3] W. Zhai, Z. Han, Z. Chen, L. Ling, S. Zhu, Train–track–bridge dynamic interaction: a state-of-the-art review, Veh. Syst. Dyn. 57 (2019) 984–1027.
[4] D.J. Thompson, Railway noise and vibration: mechanisms, modelling and means of control, Elsevier, 2009.
[5] D.J. Thompson, C.J.C. Jones, Review of the modelling of wheel/rail noise generation, J. Sound Vib. 231 (2000) 519–536.
[6] Y.-K. Luo, S.-X. Chen, L. Zhou, Y.-Q. Ni, Evaluating railway noise sources using distributed microphone array and graph neural networks, Transp. Res. Part D: Transp. Environ. 107 (2022), 103315.
[7] D.J. Thompson, G. Squicciarini, B. Ding, L. Baeza, A state-of-the-art review of curve squeal noise: Phenomena, mechanisms, modelling and mitigation, in: Notes Numer. Fluid Mech. Multidiscip. Des., Springer, Cham, 2018, pp. 3–41.
[8] R. Stefanelli, J. Dual, E. Cataldi-Spinola, Acoustic modelling of railway wheels and acoustic measurements to determine involved eigenmodes in the curve squealing phenomenon, Veh. Syst. Dyn. 44 (2006) 286–295.
[9] G. Xie, P.D. Allen, S.D. Iwnicki, A. Alonso, D.J. Thompson, C.J.C. Jones, Z. Y. Huang, Introduction of falling friction coefficients into curving calculations for studying curve squeal noise, Veh. Syst. Dyn. 44 (2006) 261–271.
[10] Y.K. Luo, L. Zhou, Y.Q. Ni, Towards the understanding of wheel-rail flange squeal: In-situ experiment and genuine 3D profile-enhanced transient modelling, Mech. Syst. Sig. Process. 180 (2022), 109455.
[11] X. Li, D. Yang, G. Chen, Y. Li, X. Zhang, Review of recent progress in studies on noise emanating from rail transit bridges, J. Modern Transport. 24 (2016) 237–250.
[12] Z. Tao, J.A. Moore, M. Sanayei, Y. Wang, C. Zou, Train-induced floor vibration and structure-borne noise predictions in a low-rise over-track building, Eng. Struct. 255 (2022), 113914.
[13] C. Mellet, F. Létourneaux, F. Poisson, C. Talotte, High speed train noise emission: Latest investigation of the aerodynamic/rolling noise contribution, J. Sound Vib. 293 (2006) 535–546.
[14] A. Gidlöf-Gunnarsson, M. Ögren, T. Jerson, E. Öhrström, Railway noise annoyance and the importance of number of trains, ground vibration, and building situational factors, Noise Health 14 (2012) 190–201.
[15] D.J. Thompson, G. Kouroussis, E. Ntotsios, Modelling, simulation and evaluation of ground vibration caused by rail vehicles, Veh. Syst. Dyn. 57 (2019) 936–983.
[16] C. Zou, J.A. Morre, M. Sanayei, Z. Tao, Y. Wang, Impedance model of train-induced vibration transmission across a transfer structure into an over track building in a metro depot, J. Struct. Eng. (2022).
[17] B. Hemsworth, Recent developments in wheel/rail noise research, J. Sound Vib. 66 (1979) 297–310.
[18] D.J. Thompson, on the Relationship Between Wheel and Rail Surface Roughness and Rolling Noise, J. Sound Vib. 193 (1996) 149–160.
[19] D.J. Thompson, Predictions of acoustic radiation from vibrating wheels and rails, J. Sound Vib. 120 (1988) 275–280.
[20] D.J. Thompson, P.E. Gautier, Review of research into wheel/rail rolling noise reduction, Proc. Inst. Mech. Eng., Part F: J. Rail Rapid Transit. 220 (2006) 385–408.
[21] M.F. Harrison, D.J. Thompson, C.J.C. Jones, The calculation of noise from railway viaducts and bridges, Proc. Inst. Mech. Eng., Part F: J. Rail Rapid Transit. 214 (2000) 125–134.
[22] F. Poisson, F. Margiocchi, The use of dynamic dampers on the rail to reduce the noise of steel railway bridges, J. Sound Vib. 293 (2006) 944–952.
[23] L. Liang, X. Li, Y. Sun, Z. Gong, R. Bi, Measurement research on vibro-acoustic characteristics of large-span plate-truss composite bridge in urban rail transit, Appl. Acoust. 187 (2022), 108518.
[24] X.D. Song, Q. Li, D.J. Wu, Study on structure-borne low-frequency noise from rail transit bridges using inverse boundary element method, Procedia Eng. 199 (2017) 1380–1385.
[25] L. Song, X. Li, J. Zheng, M. Guo, X. Wang, Vibro-acoustic analysis of a rail transit continuous rigid frame box girder bridge based on a hybrid WFE-2D BE method, Appl. Acoust. 157 (2020), 107028.
[26] X. Zhang, X. Li, L. Song, B. Su, Y. Li, Vibrational and acoustical performance of concrete box-section bridges subjected to train wheel-rail excitation: Field test and numerical analysis, Noise Control Eng. J. 64 (2016) 217–229.
[27] Q. Liu, X. Li, X. Zhang, Y. Zhou, Y.F. Chen, Applying constrained layer damping to reduce vibration and noise from a steel-concrete composite bridge: An experimental and numerical investigation, J. Sandw. Struct. Mater. 22 (2020) 1743–1769.
[28] X. Song, Q. Li, Numerical and experimental study on noise reduction of concrete LRT bridges, Sci. Total Environ. 643 (2018) 208–224.
[29] D.J. Köstli, K.P., Jones, C.J.C., Thompson, Experimental and Theoretical Analysis of Railway Bridge Noise Reduction Using Resilient Rail Fasteners in Burgdorf, Switzerland, in: Noise Vib. Mitig. Rail Transp. Syst. Notes Numer. Fluid Mech. Multidiscip. Des., Springer, Berlin, Heidelberg, 2008.
[30] S. Kirkup, The Boundary Element Method in Acoustics, Integrated Sound Software, 2000.
[31] X. Liu, N. Zhang, Q. Sun, Z. Wang, C. Zang, An efficient frequency domain analysis method for bridge structure-borne noise prediction under train load and its application in noise reduction, Appl. Acoust. 192 (2022).

[32] Q. Li, Y.L. Xu, D.J. Wu, Concrete bridge-borne low-frequency noise simulation based on traintrackbridge dynamic interaction, J. Sound Vib. 331 (2012) 2457–2470.
[33] Q. Liu, D.J. Thompson, P. Xu, Q. Feng, X. Li, Investigation of train-induced vibration and noise from a steel-concrete composite railway bridge using a hybrid finite element-statistical energy analysis method, J. Sound Vib. 471 (2020), 115197.
[34] F. Nentwich, T. Bartosch, SEA vehicle model for rolling- and engine noise Exterior Sound Field, in: Proc. Int. Conf. Acoust., Rotterdam, 2009.
[35] H.P. Lee, K.M. Lim, S. Kumar, Noise assessment of elevated rapid transit railway lines and acoustic performance comparison of different noise barriers for mitigation of elevated railway tracks noise, Appl. Acoust. 183 (2021), 108340.
[36] P.A. Morgan, D.C. Hothersall, S.N. Chandler-Wilde, Influence of shape and absorbing surface - A numerical study of railway noise barriers, J. Sound Vib. 217 (1998) 405–417.
[37] S. Ouakka, O. Verlinden, G. Kouroussis, Railway ground vibration and mitigation measures: benchmarking of best practices, Railw. Eng. Sci. 30 (2022) 1–22.
[38] Z. Cao, T. Guo, Z. Zhang, A. Li, Measurement and analysis of vibrations in a residential building constructed on an elevated metro depot, Measurement 125 (2018) 394–405.
[39] C. Li, W. Liu, R. Liang, Identification of vertical wheel-rail contact force based on an analytical model and measurement and its application in predicting ground-borne vibration, Measurement 186 (2021), 110182.
[40] A. Garinei, G. Risitano, L. Scappaticci, F. Castellani, An optimized method to evaluate the performance of trench isolation for railway-induced vibration, Measurement 94 (2016) 92–102.
[41] B. Tutmez, A. Baranovskii, Quantifying uncertainty in railway noise measurement, Measurement 137 (2019) 1–6.
[42] P.J. Remington, Wheel/rail noise-Part IV: Rolling noise, J. Sound Vib. 46 (1976) 419–436.
[43] T. Xin, S. Wang, L. Gao, H. Huo, Y. Ding, P. Wang, P. Chen, P. Liu, Field measurement of rail corrugation influence on environmental noise and vibration: A case study in China, Measurement 164 (2020), 108084.
[44] Y. Sun, W. Zhai, Y. Guo, A robust non-Hertzian contact method for wheel–rail normal contact analysis, Veh. Syst. Dyn. 56 (2018) 1899–1921.
[45] E.A.H. Vollebregt, Survey of programs on contact mechanics developed by J.J. Kalker, Veh. Syst. Dyn. 46 (2008) 85–92.
[46] X. Zhao, Z. Wen, M. Zhu, X. Jin, A study on high-speed rolling contact between a wheel and a contaminated rail, Veh. Syst. Dyn. 52 (2014) 1270–1287.
[47] K. Knothe, A. Groß-Thebing, Short wavelength rail corrugation and non-steady-state contact mechanics, Veh. Syst. Dyn. 46 (2008) 49–66.
[48] D.N. Higa, E.J. Kina, A. Gay Neto, Wheelset-rail mechanical model for a steady-state dynamic condition and prediction of rolling contact fatigue locci, Veh. Syst. Dyn. 60 (2022) 281–308.
[49] S. Jiang, P.A. Meehan, D.J. Thompson, C.J.C. Jones, Railway rolling noise prediction: Field validation and sensitivity analysis, Int. J. Rail Transport. 1 (2013) 109–127.
[50] D.J. Thompson, Wheel-rail noise generation, part IV: Contact zone and results, J. Sound Vib. 161 (1993) 447–466.
[51] P. Shackleton, S. Iwnicki, Comparison of wheel-rail contact codes for railway vehicle simulation: An introduction to the Manchester Contact Benchmark and initial results, Veh. Syst. Dyn. 46 (2008) 129–149.
[52] ISO 3095 Railway applications-Acoustics-Measurement of noise emitted by railbound vehicles, 2005.
[53] Q. Li, D.J. Wu, Analysis of the dominant vibration frequencies of rail bridges for structure-borne noise using a power flow method, J. Sound Vib. 332 (2013) 4153–4163.
[54] Q. Li, D.J. Thompson, Prediction of rail and bridge noise arising from concrete railway viaducts by using a multilayer rail fastener model and a wavenumber domain method, Proc. Inst. Mech. Eng., Part F: J. Rail Rapid Transit. 232 (2018) 1326–1346.
[55] X. Li, X. Zhang, Z. Zhang, Q. Liu, Y. Li, Experimental research on noise emanating from concrete box-girder bridges on intercity railway lines, Proc. Inst. Mech. Eng., Part F: J. Rail Rapid Transit. 229 (2015) 125–135.
[56] L. Song, K. Gao, Q. Liu, L. Zhang, Q. Feng, W. Guo, Acoustic performance of near - rail low - height noise barriers installed on suburban railway bridges, Environ. Sci. Pollut. Res. (2022).
[57] L. Man, Y. Xiang, C. Xuyong, Research and Development of Acoustic Material for Simulating Ground Absorption, Audio Eng. 38 (2014) 5–11.
[58] X. Zhang, R. Liu, Z. Cao, X. Wang, X. Li, Acoustic performance of a semi-closed noise barrier installed on a high-speed railway bridge: Measurement and analysis considering actual service conditions, Measurement 138 (2019) 386–399.
[59] J. Zheng, X. Li, X. Qiu, D. Liu, S. Zhao, Y. Qian, Field study on train-induced aerodynamic pressure near the entrance of fully enclosed sound barriers, Veh. Syst. Dyn. 1–18 (2022).
[60] J. Zheng, X. Li, X. Zhang, R. Bi, X. Qiu, Structure-borne noise of fully enclosed sound barriers composed of engineered cementitious composites on high-speed railway bridges, Appl. Acoust. 192 (2022), 108705.
[61] J. Zheng, Q. Li, X. Li, Y. Luo, Train-Induced Fluctuating Pressure and Resultant Dynamic Response of Semienclosed Sound Barriers, Shock Vib. 2020 (2020).